1949

FIBER BUNDLE MODELLING OF FAILURE PHENOMENA

Thesis for the Degree of Doctor of Philosophy (PhD)

Attia Batool

Supervisor: Dr. Kun Ferenc

University of Debrecen
Doctoral Council of Natural Sciences and Information Technology
Doctoral School of Physics
Debrecen 2022

Hereby I declare that I prepared this thesis within the Doctoral Council of Natural Sciences and Information Technology, Doctoral School of Physics, University of Debrecen in order to obtain a PhD Degree in Natural Sciences at Debrecen University.
The results published in the thesis are not reported in any other PhD theses.

Debrecen, 2022.

.....
Attia Batool
Doctoral candidate

Hereby, I confirm that Attia Batool candidate, conducted her studies with my supervision within the Physical Methods in Interdisciplinary Researches Doctoral Program of the Doctoral School of Physics between 2018 and 2022. The independent studies and research work of the candidate significantly contributed to the results published in the thesis.
I also declare that the results published in the thesis are not reported in any other theses.
I support the acceptance of the thesis.

Debrecen, 2022.

.....
Dr. Kun Ferenc
Supervisor

FIBER BUNDLE MODELLING OF FAILURE PHENOMENA

Dissertation submitted in partial fulfilment of the requirements for the doctoral (PhD) degree in **Physics**

Written by **Attia Batool** certified Physicist

Prepared in the framework of Doctoral School of Physics of the University of Debrecen

Physical Methods in Interdisciplinary Researches programme

Dissertation advisor: **Dr. Kun Ferenc**

The official opponents of the dissertation:

Dr. ....
Dr..... .....

The evaluation committee:

Chairperson: Dr..... .....
Members: Dr..... .....
Dr..... .....
Dr..... .....
Dr..... .....

The date of the dissertation defence: ..... 20 ...

Contents

1 Chapter

Introduction

In the framework of my PhD research I investigated failure phenomena emerging in complex systems made up of a large number of interacting elements. From the mechanically induced fracture of solid bodies [1–3] through the breakdown of traffic in urban areas [24, 25] to the blackout of high voltage power grids [4, 6–9], a large diversity of failure phenomena can be mentioned which have interesting common features. First of all, the local failure of an element of the system can trigger further failure events due to the load redistribution over the remaining intact elements. Together with the constraint of load conservation this load sharing mechanism can induce cascades of failures which may spread over a large fraction of the system eventually leading to global failure. The process of spreading and the overall stability of the system is substantially affected by the degree of disorder of the load bearing capacity of the individual elements [2]. Disorder usually reduces the ultimate strength of the system [11, 33], however, at the micro-level, it can help to arrest propagating failure avalanches, hence, increasing the damage tolerance of the system [1–3, 12, 13, 33]. Recent investigations have revealed that such failure phenomena are characterized by scaling laws both on the macro- and micro-scales and their characteristics exhibit a high degree of robustness against specific details of the failing

system [33]. This lead to the emergence of the idea that the theory of phase transitions and critical phenomena provide the adequate framework for the description of such failure phenomena. Most notably, for the fracture processes of heterogeneous materials the phase transition description proved to provide new insights [2, 12–16, 33].

To study failure phenomena, the capabilities of analytical calculations are rather limited, hence, the computer simulation of discrete models is indispensable. Among the theoretical approaches, in particular for fracture phenomena, the fiber bundle model (FBM) has proven to be the most successful modelling framework because it grasps the key mechanisms of the fracture of heterogeneous materials yet being so simple to provide analytic solutions in certain limiting cases [15–18, 20–22].

My PhD research is focused in two main directions. For a deeper understanding of phase transition analogy of fracture phenomena I investigated the impact induced perforation of a solid bar [23]. For simplicity, I constructed a model of a bar shaped specimen in such way that the bar is made up of two rigid blocks glued together by an elastic interface. The interface is discretized in terms of a bundle of parallel fibers which have disordered strength and break when over-stressed. Impact loading in the middle causes deflection of the bar accompanied by the cracking of the interface. Slowly increasing the impact energy, I showed that perforation, i.e. the breakthrough of the bar, occurs at a critical energy analogous to the continuous phase transitions. I determined the critical exponents of the transition and analyzed the role of degree of disorder on the behaviour of the system. The results obtained form the basis of my first thesis point [23].

In its basic setup, a fiber bundle model containing a set of parallel fibers arranged on a regular square lattice [17, 22]. Under a gradually increasing applied load the fibers undergo irreversible failure when their local load exceeds their random breaking threshold. The load of the failed fiber is redistributed over the surviving intact fibers. Recently, two

limiting cases of load sharing have been intensively studied, both of which are of high practical relevance: in equal load sharing (ELS) case, all unbroken fibers get the same fraction of load regardless of their distance from the failed fiber, while in localized load sharing (LLS) case the load of broken element is equally redistributed to its intact neighbors only [15, 16, 18, 20, 21]. In each case the load increments can trigger further breaking such that a single broken fiber can trigger an entire avalanche of failure events. Because of the generic nature of this failure spreading mechanism, dfibers of the model can easily be replaced by roads carrying traffic [24, 25] flow channels [26], or electric power stations [4, 6–9] on a high voltage transmission grid, making FBMs a basic modelling framework for cascading failure with widespread applications on complex networks [27].

I used the fiber bundle model of breakdown phenomena as a general modelling framework of cascading failure to investigate how the statistical features of failure cascades, and the overall performance of the damaged system depend on the structure of underlying load transmission network [28]. In particular, for my second thesis point I studied how the interplay of network structure and the degree of disorder of the nodes' strength affects the failure dynamics. I showed that a transition occurs from the localized to mean field behavior of FBMs as the network of load transmitting connections is gradually randomized starting from a regular lattice. However, the degree of strength disorder of nodes has a substantial effect on the transition. Most notably, I demonstrated that the transition is limited to a well-defined range of disorder with a threshold value below which randomization is disadvantageous for the overall performance of the system [28].

For the third thesis point I investigated how the interplay of the network structure and the degree of disorder of the nodes' strength affects the temporal evolution of failure cascades [29]. I showed that the size and duration of cascades both are power law distributed on all network

topologies considered. Most notably, I demonstrated that the temporal evolution of cascades is described by a parabolic profile with a right handed asymmetry which implies that cascades start slowly then accelerate and eventually stop suddenly. The degree of asymmetry proved to be characteristic for the network topology gradually decreasing with increasing structural randomness. The consistency of the results was supported by a scaling analysis valid at any degree of disorder of the strength of nodes [29].
In my studies, I have used the approaches and tools of statistical physics, phase transitions and critical phenomena, the physics of complex systems, and network science. My investigations are purely theoretical, starting from the general fiber bundle model I constructed efficient modelling approaches for dynamic fracture of a bar and for cascading failure phenomena on complex networks. I performed computer simulations on the supercomputer of the University of Debrecen. I developed both the simulation codes and the data evaluation programs of numerical measurements. In my thesis, after summarising the literature and modelling methods that motivated my research, I will state my objectives and present my results in three separate chapters.

2 Chapter

Failure phenomena in complex systems

In the framework of my PhD research I investigated failure phenomena emerging in complex systems which are composed of a large number of interacting elements. This chapter gives a review of the scientific literature focusing on the role of disorder in fracture phenomena and on the microscopic mechanism of cascading failure in complex systems. It also presents the basic concepts of phase transitions and complex networks, highlighting the significant theoretical and experimental achievements that form the basis of my own research.

2.1 Fracture of heterogeneous materials

When a slowly increasing mechanical load is applied on a solid body, it falls apart into two or more pieces at a critical value of the load [3]. This process is termed as fracture. In addition to material characteristics, the fracture process and its outcome strongly depends on how the external load is applied. If a body is subjected to a force greater than its critical load, a fracture will occur suddenly and in a short time. However, under a smaller, so-called sub-critical constant load fracture proceeds slowly

and takes a long duration. There are two types of sub-critical fracture: *creep fracture* when the material is subjected to the limit of a constant load over a long period of time, and *fatigue fracture* when it is subjected to a time-varying load. Dynamic fracture occurs when rapid loading is applied but the boundary conditions ensure that a single growing crack is generated which advances at a high speed.
In daily life fracture phenomena is encountered frequently in different aspects. For example, splitting of log with wedge, failure of bridges, pipes, railway tracks etc. Also some catastrophic structural failures resulting loss of life have occurred, which substantially lead to the development of fracture mechanics. The earliest studies on fracture mechanics was done by Griffith [30]. He proposed his classical condition for the propagation of cracks in brittle materials under quasi-static or static conditions. His results were in agreement with experimental studies of brittle solids. Irwin modified Griffith's theory [31] including the plastic zone growing at the crack tip, while Bazant [32] generalized the theory to the fracture of quasi brittle materials.

2.1.1 Effect of heterogeneity on fracture

We are familiar with the fact that in solids fracture occurs at much lower stresses than the estimated stress from the solid state physics of crystalline structures [3]. Mostly in materials the ratio of estimated to observed fracture strength is about 2 to 3 orders of magnitude. This discrepancy can be resolved easily by assuming that the stress field inside the specimen can not be homogeneous because of the disordered meso- or microscale structure [3, 33]. Depending on the relevant length scales, disorder can appear in various different forms: On the microscopic level, examples of disorder are vacancies, inclusions and dislocations. Larger scale disorder are present in the structure of granular materials or composites like concrete or ceramics. Migration of dislocations, formation and healing of micro-cracks, diffusion of interstitials etc. are examples of

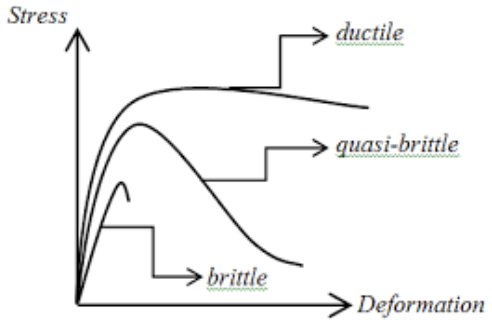

Figure 2.1: Stress-strain curves of different types of disordered materials: in case of brittle materials failure occurs already in the linear regime; for quasi-brittle materials the curve has a maximum where failure occur under a stress controlled loading; for ductile materials a monotonically increasing functional form is obtained indicating that fracture advances slowly and failure is reached after a considerable amount of plastic deformation [35].

dynamic disorder. Inside a loaded specimen in the presence of disorder, stress accumulates around weak spots, initiating the fracture there. As the load increases, further cracks nucleate and existing cracks grow so that the material fails globally as a result of this stable damage accumulation process [34]. Hence, in the presence of weak regions, a loaded specimen becomes unstable and fails at lower loads, i.e. the presence of disorder generally reduces the tensile strength. On the other hand, in the limit of zero disorder, the global failure is preceded only by a small damage, resulting in an abrupt failure already at a low deformation.

Depending on the macroscopic response of disordered materials, two main types of fracture are distinguished: *quasi-brittle fracture*, when the stress-strain curve of the solid has a usually quadratic maximum, where it suddenly fails under stress controlled loading, and *ductile fracture* when fracture slowly proceeds and a significant plastic deformation accumulates before final failure (see Fig. 2.1). Moreover, the ultimate strength of

heterogeneous materials fluctuates as a consequence of disorder, so it can be characterized by a probability distribution. For disordered, quasi-brittle materials, the Weibull distribution proved to be the most suitable distribution for the quantitative description of the stochastic strengths. Laboratory measurements have revealed that increasing the size of the specimen, the average fracture strength decreases due to the higher chance of having weaker spots in larger bodies. This so-called statistical size effect has to be taken into account in engineering design of large scale constructions such as buildings or water dams.

2.1.2 Crackling noise

The stable cracking of heterogeneous materials is accompanied by the emission of acoustic noise, which can be recorded by sensitive microphones. Measuring this crackling noise is extremely important to understand the evolution fracture phenomena, as it gives useful information on the microscopic process of crack initiation and propagation, and on the overall behaviour of the system as it approaches ultimate failure.
The intensity of the crackling activity depends on materials' degree of disorder [10]. Materials with low disorder usually fail as a result of sudden formation and fast propagation of a single crack. However, fracture of highly disorder material occurs progressively: under an increasing load first nucleation of un-correlated micro-cracks takes place throughout the volume of material at points of high load concentration. Further increasing the load, existing micro-cracks keep growing along with new crack nucleation events. A single growing crack keeps localizing while reaching the critical stress, along which the sample falls apart. Due to disorder, the nucleation and growth steps occur in a jerky way giving rise to crackling avalanches which generate acoustic pulses. This is illustrated in Fig. 2.2(a) where the noise emitted during tearing a sheet of paper was measured. Crackling noise time series contain a huge

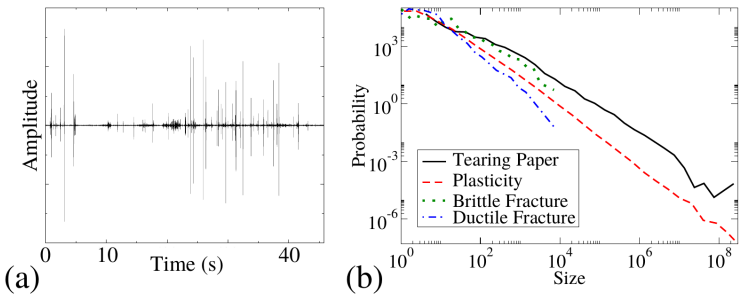

Figure 2.2: (*a*) Crackling noise generated by fracturing paper. The amplitude of acoustic events in plotted as a function of time as a sheet of papered is teared apart by slowly increasing its deformation at a constant rate. (*b*) The probability distribution of the size (magnitude) of acoustic events in four different experiments: paper tearing, plastic flow of ice, brittle fracture of concrete and ductile fracture of steel [36].

amount of information about the evolution of loaded systems. In the simplest case one can analyze the statistics of the characteristic quantities of individual pulses such as their energy E and duration T. Experimental and theoretical investigations showed that the probability distributions $p(E)$ and $p(T)$ exhibit a scale free behaviour, i.e. they can be well approximated by power laws

$$p(E) \sim E^{-\alpha}, \tag{2.1}$$

$$p(T) \sim T^{-\beta}, \tag{2.2}$$

where the value of the exponents have a high robustness against material properties. Examples of the energy distribution $p(E)$ of crackling events are presented in Fig. 2.2 measured during tearing paper, brittle fracture of concrete, ductile fracture of steel, and plastic flow of ice specimens [36–39]. A large amount of laboratory experiments confirmed the high degree of robustness of the exponents of the scale free statistics of the characteristic quantities of crackling events against materials' details.

2.2 Networks

There exists a large variety of physical, technological, biological, or social systems composed of a large number of constituents, where the functioning of the system is governed by the pattern of connections of the elements. These connections represent interactions, which may occur, for instance, in the form of load redistribution in the case of a solid body under mechanical load, can be established by social contacts of individuals, or may arise through the flow of information or energy between the elements of the system. Since failure propagation is strongly affected by the structural features of the underlying interaction network, here we briefly review the most important basic notions of network science.

2.3 Some basic notions of network science

A simple network is composed of nodes connected by links in such a way that neither multiple links, nor loops (self links) occur. Links can carry a weight representing some additional information on the connection such as the real physical distance, or the strength of coupling of the elements of the system. In such a case the network is called weighted, otherwise it is unweighted. Links can be directed indicating, for instance, the direction of the flow of some quantities or a hierarchy of nodes. In my own research I focused on undirected and unweighted networks where links are either present or not. For an example of a simple network see Fig. 2.3.

One of the most important characteristic quantity of nodes in a network is the degree k, which is the number of immediate neighbors connected by direct links to it. In a simple network of N nodes the total number of links L can be expressed in terms of the node degrees k_i $(i = 1, \ldots, N)$ as $L = 1/2 \sum_{i=1}^{N} k_i$. The degree of nodes is typically a fluctuating quantity

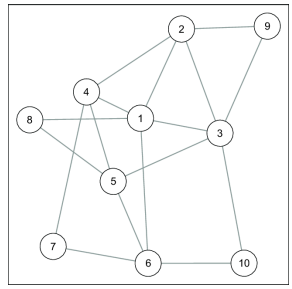

Figure 2.3: A simple graph of 10 nodes connected by 17 links [40].

so that networks are characterized by the probability distribution $\rho(k)$ of their nodes. In real networks commonly occurring degree distributions are the Poisson distribution

$$\rho(k) = \frac{e^{-\langle k \rangle} \langle k \rangle^k}{k!}, \tag{2.3}$$

the exponential distribution

$$\rho(k) \sim e^{-k/d}, \tag{2.4}$$

and the power law distribution

$$\rho(k) \sim k^{-\gamma}, \quad \gamma > 1, \tag{2.5}$$

where d and γ are parameters of the distributions, and $\langle k \rangle$ denotes the average degree. Networks of different degree distributions are illustrated in Fig. 2.4.

The local connectivity of the network can be characterized by the clustering coefficient C, which is the probability that two neighbours of a node are neighbours of each other too. The local clustering coefficient C_i of a node i in a network can be obtained as

$$C_i = \frac{k_i}{k_i(k_i - 1)/2}. \tag{2.6}$$

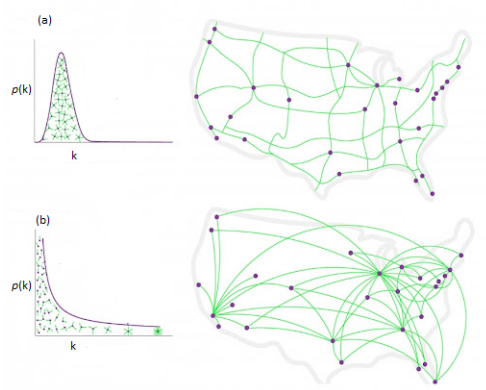

Figure 2.4: Examples of networks of different degree distributions. (a) Network of the US highway system, where nodes are cities which are linked by highway connections. The degree distribution can be well approximated by a Poissonian. (b) The US airline network has a power law degree distribution. Here the nodes are airports which are linked if there exists a direct flight between them [41].

The arithmetic average of C_i over the network provides a measure of the global connectivity of the system

$$C = \frac{1}{N} \sum_i C_i. \tag{2.7}$$

Starting from a node one can construct a path through the links of the network to another node, where the length l of the path is the number of links visited. If there exists a path between any two nodes, the network is fully connected, i.e. it has only a single component, otherwise it is composed of several components. Between two nodes there may be several possible paths, among which the length of the shortest one characterizes the separation of the two nodes. A useful measure of the extension of fully connected networks is the average path length $\langle l \rangle$ which is defined as the average of the length of shortest paths over all possible pairs of nodes. It is a very interesting feature often observed in real

networks that the average path length, i.e. the degree of separation of nodes, is much smaller than the size of the system, and if the system size is increased the average path length increases only logarithmically

$$\langle l \rangle \sim \ln N. \tag{2.8}$$

This feature is called as small world behaviour, which was first observed experimentally by Milgram. Based on his experiments he concluded that the average separation of individuals in human societies is about 6.

2.4 Classification of networks

Real networks can be classified into four basic types: technological, information, social and biological networks. Networks of a given class share similar structural properties and they can be analyzed by the same type of mathematical approaches.
Technological networks are the physical infrastructural networks that form the background of modern societies. The prime example of technological networks is the Internet which is the network of routers coupled by data transmitting connections. The internet has a power law degree distribution together with a high clustering coefficient and a small path lengths [43], confirming its small world characteristics. Telephone network is a large directed network between distant call patterns, where phone numbers are nodes and phone call is a link, direction from caller to receiver. Telephone network also shows power law degree distribution [44]. Power grid is a network of transmission lines of high-voltage that transport electric power at long distances. Local power lines of low voltage that deliver electricity to consumers are not included in this network type. Generating stations are considered as nodes of the network and the high-voltage lines are edges. Airline routes, roads and railway networks are examples of transportation networks. Sewerage lines, water, oil and gas pipelines, and paths used by parcels delivery companies and

post offices are examples of distribution networks.

Information networks are networks made up e.g. of people, or computers and procedures for collection, processing, transmission and dissemination of data. Some examples are: The world wide web is currently the biggest network with known topological information. It is a directed network where nodes are the web pages having pictures, text and other information and the hyperlinks are the edges which allow us to click our way from one page to another. In contrast to the internet, web is not the physical connection of data between computers but it is network of logical connections of information pages. World wide web is a directed network, it follows a power law degree distribution and it shows small world beviour [45]. Citation networks are formed in such a way that papers (documents) are nodes and there is a directed link from paper X to Y, if X cites Y. In this network incoming degree distribution shows a power law behaviour, whereas outgoing degrees have an exponential distribution [46].

Social networks are composed of people or group of people who have some kind of social interaction between them such as friendship and business relationship etc. People in the network are considered as nodes and interaction (friendship, love, common political opinion) between them are links. *Actor collaboration network* is an example of social network. Actors are vertices in this network and the link is common between two vertices if corresponding actors appeared together in a movie [47].

Biological networks represent the type of interaction between biological elements, which can occur at different levels in ecosystems. Most common examples of biological networks are metabolic network, food web, genetic regulatory network, protein-protein interaction network, and neural networks etc. *Protein-protein interaction network* mathematically represents physical contacts that occur between binding regions in proteins. They exhibit small world properties with a high clustering coefficient. Degree of this network follows Gaussian distribution [48].

2.5 Network Models

To understand the emergence of the structural features of different types of real networks several mathematical models have been proposed. Here a short summary of network models is presented highlighting those approaches which were extensively used in my own research.

2.5.1 The random network model

The structure of real networks has an inherent randomness that's why the random network or Erdős-Rényi model is a usual starting point of investigations. A random network comprises of N number of nodes which are linked with probability p. Since each of the $N(N-1)/2$ links is present with probability p, the actual number of links L fluctuates around the average $\langle L \rangle$ obtained as

$$\langle L \rangle = p\frac{N(N-1)}{2}. \tag{2.9}$$

Similarly, the average node degree follows as

$$< k >= p(N-1), \tag{2.10}$$

where $(N-1)$ is the maximum number of links that a node can have in a random network. The degree distribution of random networks is binomial which tends to a Poisson distribution Eq. (2.3) in the limit of large network sizes. An example of real networks with Poissonian degree distribution is the US highway network presented in Fig. 2.4 (a), where nodes are cities which are connected by a link, if a direct highway connection exists between them [49]. An important property of the Poissonian distribution is that it is relatively narrow so that most of the nodes have degrees k in the vicinity of the average $\langle k \rangle$. In the example it means that there are no cities which have an order of magnitude more highway connections than the others.

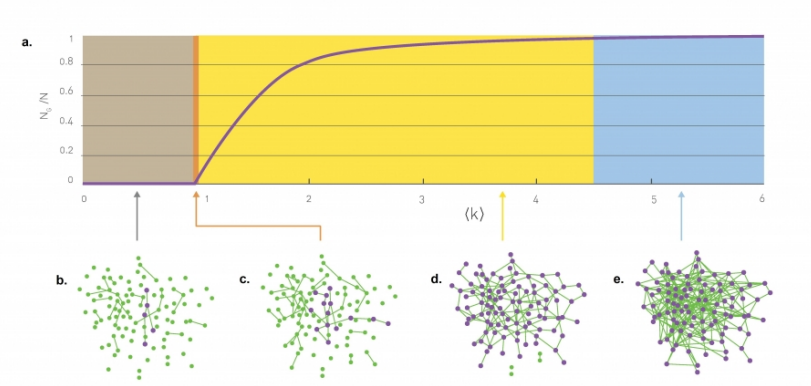

Figure 2.5: Evolution of random networks with increasing average degree $\langle k \rangle$. The size of the largest component is presented as a function of $\langle k \rangle$. The giant component occurs at $\langle k \rangle = 1$. Further increasing $\langle k \rangle$ the network becomes fully connected and then it becomes a complete graph where all possible links are present [49].

Of curse, the structure of random networks strongly depend on the value of the connection probability p. At low values of p the network is composed of several connected clusters called components where even the largest one is significantly smaller than the entire size of the network N. As p is increased the size of the components increases, while their number gets reduced. When p exceeds a threshold value a so called giant component emerges which comprises a finite fraction of the network even in the limit of large network sizes, or in other words the ratio N_G/N (where N_G is size of the largest component), remains finite in the limit $N \to \infty$. Erdős and Rényi showed that the giant component appears when each node has at least one neighbor on average

$$\langle k \rangle = 1. \tag{2.11}$$

The result also implies that for larger networks the giant component emerges at a lower value of the probability $p = 1/(N-1) \approx 1/N$ [49]. To

be able to compare networks of different sizes, it is advantageous to present the evolution of random graph using $\langle k \rangle$ as an independent variable instead of the connection probability p. Figure 2.5 presents the relative size of the giant cluster N_G/N as a function of $\langle k \rangle$. It can be observed that below $\langle k \rangle = 1$ the network is composed is composed of a large number of small components. The giant cluster occurs at $\langle k \rangle = 1$, however, surrounded by a large number of components whose size is significantly smaller than that of the giant one. Further increasing $\langle k \rangle$ the network becomes fully connected and later on it converges to a complete graph, where all possible links are present.
Since the probability that any two nodes are connected in the network is p, the clustering coefficient of random networks does not depend on the node degree $C = p$. For real networks where p can be estimated from the average node degree, this implies a very low clustering, significantly smaller than the measured values. At the same time, the randomness implies the presence of long range connections which reduce the average path length yielding $\langle l \rangle = \frac{\ln N}{\ln \langle k \rangle}$. Hence, the average path length logarithmicaly increases with the size of the network N and gets smaller when the average degree is increased. Comparing to real networks practically the low average path length, i.e. the small world nature is the only feature of random networks which agrees with the results of measurements [50].

2.5.2 Watts-Strogatz model

Two most important properties of real world networks are the high clustering coefficient and the short average path length (small world effect) [50]. The random network model and regular lattices, often used in physics, capture one of these features but not both at a time. This difficulty leads to construct a composite of these two models, proposed by Watts and Strogatz in 1998, that simultaneously display both short path length and high clustering coefficient [51].

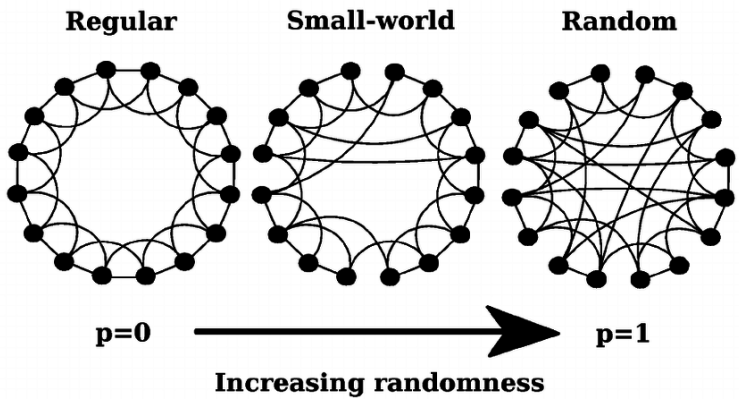

Figure 2.6: Illustration of the Watts-Strogatz model: starting from a regular network where each node is connected to its four nearest neighbors along a ring, a fraction p of links is rewired between randomly selected nodes hence introducing long range connections in the system. In the limit $p \to 1$ of the rewiring probability a random network is obtained [51].

Starting from a regular ring graph shown in Fig. 2.6, Watts and Strogatz proposed to randomly rewire links to any other position. There are two versions of the Watts-Strogatz (WS) model: in the earlier one additional links are introduced between randomly selected sites, keeping the original links of the regular lattice. In this model isolated clusters are not formed, which facilitates the analysis of the network properties[44]. The other version, called the original Watt-Strogatz model, is the one in which the original links are removed with probability p and get re-established between randomly selected sites. The basic algorithm of the model is following: *(i) Start with order*: The model construction starts from a regular graph of N nodes, which is a ring graph in the original WS model, see Fig. 2.6(a). Each node has the same degree K, connected to its first neighbours K, or $K/2$ neighbors on each side. *(ii) Random rewiring*: Each link is rewired to a random position with probability p, excluding multiple links and self-connections. Hence $pNK/2$ number of

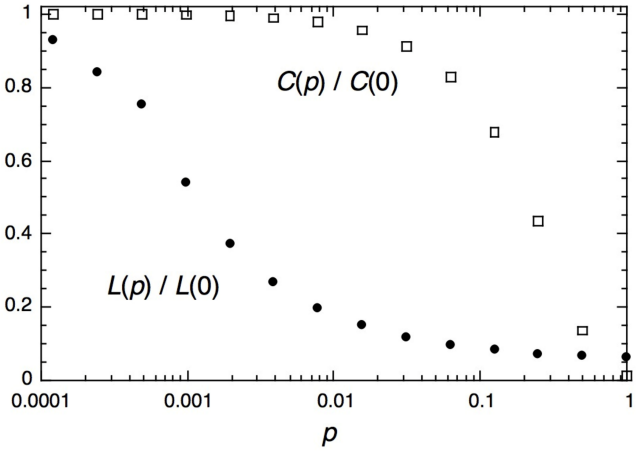

Figure 2.7: Evolution of the clustering coefficient C and of the average path length $\langle l \rangle$ of the Watts-Strogatz model as the rewiring probability p is gradually increased starting from a regular ring graph of $K = 2$ [51]. There is a range of p values where the model yields a high clustering and a short path length (small world effect) reflecting real world behaviour of networks.

long-range links are produced, connecting the nodes of different neighbourhoods. These random connections are called shortcuts. It can be seen that the WS model provides an interpolation between the regular lattice and the random network model with the rewiring probability p as a controll parameter. At $p = 0$ links are not rewired and we regain the original regular lattice, while at $p = 1$ all the links are rewired resulting in a random graph. The crucial point of the WS model is that as p increases, the high clustering of the original regular lattice is retained up to a certain value of p, while short path length also appears. Figure 2.7 provides an overview of the evolution of the clustering $C(p)$ and the average path length $\langle l \rangle (p)$ as p increases. It can be observed that there is a range of the rewiring probability p, where the model shows the real

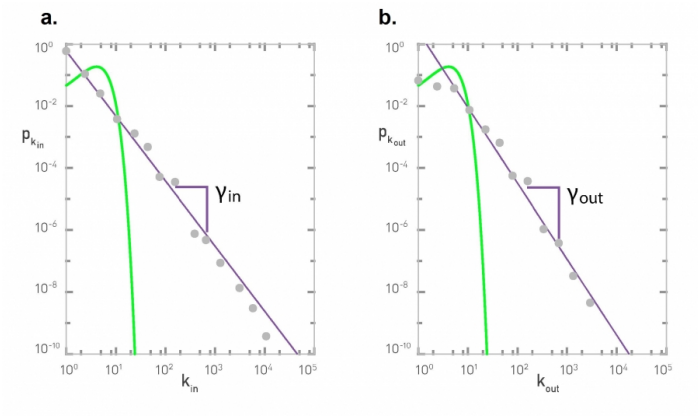

Figure 2.8: (a) incoming and (b) outgoing degree distribution of world wide web [49].

world behaviour [51].

2.5.3 Scale free Network

Real networks often have the feature that the degree of their nodes is power power law distributed given by Eq. (2.5). The value of the exponent γ typically falls between 2 and 3. As an example Fig. 2.8 shows the degree distribution of the world wide web, which is a directed networks, hence, the distribution of the number of the incoming and outgoing links is presented separately. Both show power law behaviour over nearly three orders of magnitudes in k. The random network and WS models failed to reproduce this property of real networks. Barabási showed that two features, i.e. the continuous growth of networks and the preferential attachment mechanism are responsible for the emergence of the scale free behaviour [41, 42]. This means that as the network is growing new nodes get connected to the already existing ones with a probability proportional to their current degree [42]. The scale free nature implies the existence of hubs in the networks, i.e. nodes with a

high degree, much larger than the average degree, are present in the network with a considerable probability. Hubs create short cuts, hence, scale free networks exhibit the small world behaviour. In my own research I focused on WS networks including the limiting case of completely random networks, since they are relevant for the understanding of failure propagation on technological networks.

2.6 Networks in failure phenomena

During the past two decades network science has gained widespread applications in complex systems, revealing novel, before hidden aspects of their dynamics and statistical features [50, 52]. The investigation of failure phenomena, including the fracture of heterogeneous materials, the emergence of earthquake sequences, furthermore, the failure of technological systems such as power grids, also profited from the network approach. Here a brief summary of the application of network science in the description of failure phenomena is presented, which served as a motivation of my own research.

2.6.1 Complex networks of earthquake

Even today lots of damages and causalities are caused by earthquakes, so that the understanding of the emergence of earthquakes still has a primary importance. Earthquakes form a complex spatial-temporal sequence of events caused by the movement of faults in Earth's crust. Figure 2.9 (a) shows large scale fracturing events in Chile, i.e. an earthquake map with positions of epicenters having magnitude greater than 4. Earthquakes exhibit complex correlations in magnitude, space and time. Coupled to main shocks with large magnitude, often a series of earthquakes appear, additionally, sometimes a main shock is preceded by a few precursory events. Depending upon the relative position and magnitude in the space-time sequence, evens of such trails can be labeled

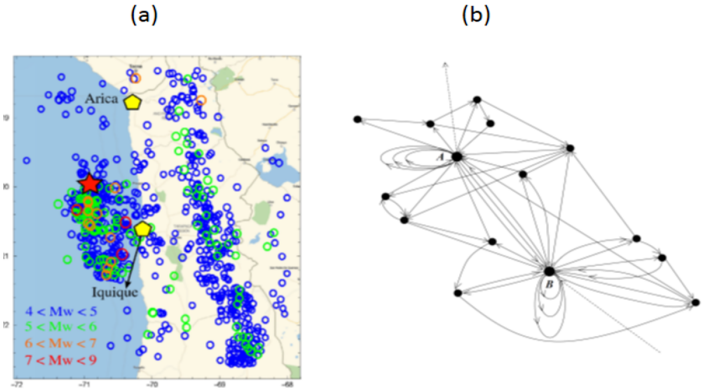

Figure 2.9: (*a*) Earthquakes in Chile with magnitude greater than 4. (*b*) Spatial-temporal sequence mapped to a graph, where nodes represent the spatial domains where the earthquake broke out, while the links indicate the triggering relation [53].

as fore-shocks, main shocks, and aftershocks.

For constructing a network model to describe an earthquake system, one needs to know what the nodes are and how they are linked together. A suitable network can reveal many useful properties of a system such as hidden correlations in the occurrence of earthquake, identification of weak spots in fault systems, and such studies can help forecasting efforts. To construct an earthquake network, two types of approaches have been used. Abe and Suzuki [54] have proposed the first approach where the geographical area under observation is divided into a large number of cubic cells. If an event occurs in a cell with any magnitude, the cell is marked as node, and a node is linked to another one if the next earthquake occurred in the other domain. Hence two consecutive events define a link between two nodes, i.e. the complex fault-fault interaction is replaced by this link. The mapping of a spatial-temporal earthquake sequence to a graph is presented in Fig. 2.9 (*b*). It can be observed that

two nodes can coincide with each other meaning that consecutive events take place in the same cell, making a loop. This construction leads to a directed network which proved to have scale free and small word properties, where main shocks act as network hubs [54]. In the second approach, an event is considered as a node by itself, which receives a link from its direct predecessor in the sequence. Outgoing links of a node point to aftershocks. Networks obtained by this approach are also scale free [55] and posses the small world property [56].

2.6.2 Fracture networks

Multiple fracture lines or planes intersecting each other form fracture network. Fractures produced in rocks when stressed due to the tectonic motions of the plates and sea ice fracture patterns are examples of three- and two-dimensional fracture networks, respectively. Of course, the two-dimensional fracture networks that can be observed on the surface of rocks are two-dimensional fingerprints of three-dimensional networks of intersecting planes. An example of a two dimensional network of fracture lines is shown in Fig. 2.10(a). Fracture and its connections have huge applications in engineering, e.g. for oil and gas production and exploration, hydrology, gas segregation etc. In particular, in carbonate petroleum reservoirs fracture networks are used for oil transportation because of their low permeability [5]. As fracture patterns in three-dimensions are intersecting fracture sheets, there is no clear concept of nodes and links for their network representation. In Ref. [58] a so called dual network representation of fracture patterns was suggested which overcomes this problem: fracture lines or planes are represented by nodes and a link is established between two nodes if the corresponding fractures intersect each other. This dual network idea is illustrated in Figs. 2.10(b, c). This representation of fracture patterns made it possible to analyze two- and three-dimensional patterns in a unified framework revealing several interesting features of the fracturing of reservoir rocks

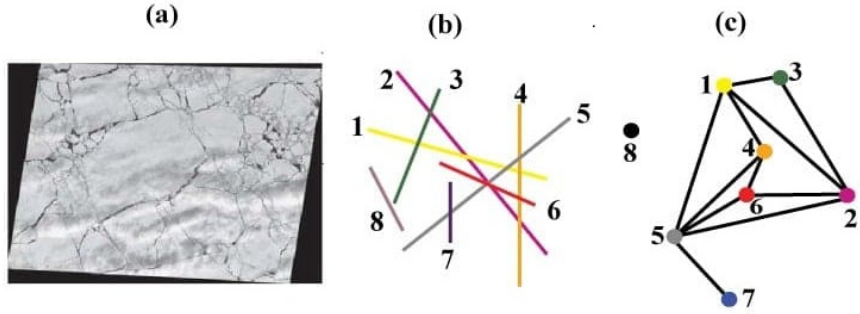

Figure 2.10: (*a*) Radar image of a sea ice fracture network taken on 28th January 1994 over the Kara sea [57]. (*b*) A schematic picture of a small network of intersecting fracture lines. (*c*) The dual network representation of the fracture pattern of (*b*) [58].

[58].

2.6.3 Cascading failure

It is a common feature of complex systems composed of a large number of elements interacting with each other that failure in one part of the system can cause further failures which then continue to spread, and as a result, the whole system may collapse loosing its functionality [59]. Examples can be mentioned in diverse systems such as the spread of epidemic on social networks [60] or the cascading activity of neural networks [61]. Cascading failure often occurs also in our technological environment, for instance, the cascading blackouts of high voltage transmission grids or the breakdown of transportation and communication systems often have a considerable economic impact [4, 9]. Most notably, in power grids, presented in Section 2.4, when due to any reason a power line fails, its power is transferred automatically to its neighboring lines, if these are able to bear the extra load then nothing

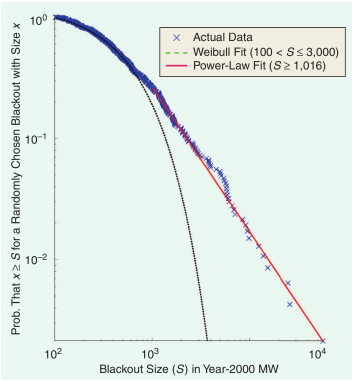

Figure 2.11: Size distribution of electric blackout events during North American blackouts from 1984 to 1998 [4].

happens [7, 9]. However, these lines will fail if they can not sustain the extra load, and redistribute their load to their neighbors. Hence, a local failure leads to a new load redistribution resulting in subsequent failure events. This step-by-step spreading of failure is called cascading failure, or failure avalanche during which a large number of power lines are overloaded and gradually collapse [65] as a consequence of a single failure event. The initial activity that stimulates the cascade can be man-made or a natural disaster. If the node carries a high load, its removal can significantly affect the load balance of the entire system and a series of overload failures are likely to happen. Figure 2.11 demonstrates that the distribution of the magnitude of power outages exhibits a power law behaviour similar to the cracking cascades.

Of course, the dynamics of spreading and the statistical features of such failure cascades strongly depend on the connectivity features of the underlying network of the interaction of components of the system, that's why network science provides the adequate framework to study these phenomena. Network studies have revealed that failure cascades occur if (i) the load bearing capacity of the nodes of the network is highly

heterogeneous. (*ii*) the node to be removed is one that carries a high load, otherwise, cascade failure is not expected [66]. There can be several possible mechanisms to trigger the spreading of failure cascades, for example: (*i*) *Load redistribution*: Load of the failed node is shifted to the neighbouring nodes leading to overloads as it has been discussed for power grids [66]. (*ii*) *Direct dependencies*: In this case if a node is collapsed then all the nodes that depend on it also become dysfunctional [67]. (*iii*) *Number of active neighbours*: Cascading failure can occur if the number of active neighbours is less or greater than a threshold [68, 69]. Cascading failures of technological networks triggered by the redistribution of load due to the local damage of interconnected elements share several common features with the fracture and failure of heterogeneous materials under external mechanical loading. As a cascade spreads through the gradual failure of overloaded elements, parts of system become permanently inactive and lose the ability to support load. The loss of load-carrying capacity, combined with the restriction of load conservation can easily lead to large scale failure events spanning a large scale fraction of system [27, 62–64]. Based on this common ground, in my research I analyzed how the cascading dynamics of fracture phenomena behaves on different network topologies.

2.7 Fracture as a phase transition

Under a gradually increasing external load heterogeneous materials undergo a damage accumulation process, and finally failure occurs at a critical load as the culmination of damage [3, 33]. The fracture process is accompanied by the emission of acoustic noise [34], which proved to have a scale free statistics, as shown earlier. The power law exponents of the distributions of the characteristic quantities of crackling noise have been found to exhibit a high robustness against materials' details [37–39]. Detailed studies also revealed that as the system approaches the critical

point time-to-failure power laws emerge [70, 71] providing a possibility of predicting the upcoming catastrophic event [10, 72, 73]. Whereas in the low disorder limit, eventual failure is preceded only by a small amount of damage, resulting in an unstable crack which induces an abrupt failure [2].
The concept that there is a connection between phase transitions and fracture phenomena has a long history [2]. Statistical physics and fracture merge in an interesting manner to understand collective phenomena in the dynamics and statistics of failure leading processes [33]. The concepts of phase transitions, universality and scaling laws seem very convincing to understand why material-specific features seem to be unrelated and why power laws appear in fracture phenomena in quantities such as avalanche size and duration, and fracture surfaces also in crack growth and nucleation dynamics [33, 74]. In particular, loaded solids are thought to be in a meta-stable state [75] becoming unstable when applied stress reaches a spinodal, hence, the failure point can be interpreted as a nucleation process in a first order phase transition [76–78]. Other studies proposed that the damage to fracture transition of materials with high disorder has analogies to continuous phase transitions because of the emergence of universal scaling laws in systems close to the critical point [79, 80]. It has also been proven recently that varying the degree of materials' disorder a transition from brittle to quasi-brittle behavior occurs, which is continuous for long range load redistribution but it becomes abrupt as disorder gets reduced [13, 14, 81, 82].

2.7.1 The concept of percolation

In the phase transition description of failure phenomena of highly disordered systems the concept of percolation turned to be especially useful. Percolation theory deals with the emergence of pathways that percolate through the lattice [86]. Consider a d-dimensional regular lattice. Lets p is the probability with which edges are present and absent

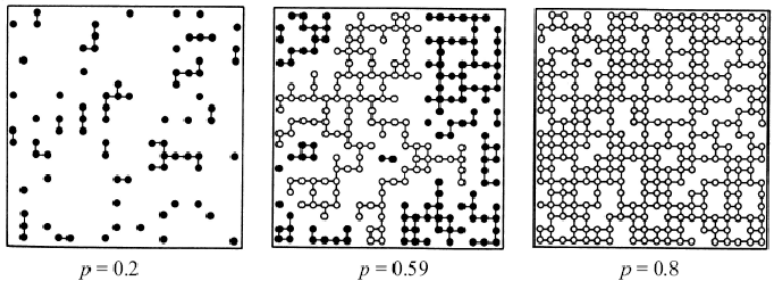

Figure 2.12: Site percolation on a square lattice with size 20×20 with random site occupied probabilities $p = 0.20,\ 0.59,\ 0.80$. Full circles represent isolated cluster sites, while open circles are for sites on giant cluster [84].

with probability $1 - p$. For small p values, a few edges are present only, so only small connected clusters of nodes can be formed, whereas at a critical probability p_c, also called percolation threshold, there appears a percolating cluster of nodes connected by edges. This cluster is called an infinite cluster, as its size diverges when size of lattice increases. So many versions of percolation are studied earlier, one discussed above is bond percolation. The well known alternative of which is site percolation, where all bonds are present and occupation probability of nodes is p. In a similar manner to bond percolation, only a few clusters of occupied nodes are present for small p, whereas at $p > p_c$ there appears an infinite cluster as shown in Fig 2.12. In the limit of very high disorder, percolation gives a good qualitative description of the evolution of the spatial structure of damage during fracture processes [1]: at early stages of the fracture process cracks randomly nucleate all over the sample. With increasing load new cracks nucleate, furthermore, old ones grow and merge forming even larger cracks. At a critical concentration cracks merge into a macroscopic fracture spanning the entire system, which causes global failure [1, 86].

When discussing the evolution of random networks with the connection

probability p at a fixed number of nodes N, it was demonstrated that there is a threshold probability p_c at which a giant cluster is formed. In terms of percolation language, p_c of random networks is equivalent to the percolation threshold of bond percolation so that the percolation transition and formation of giant cluster are indeed the same phenomenon explained in different terms [41]. Percolation has been widely studied on complex network in the context of the robustness of the system against random attacks where sites of the network are randomly removed (an active node is randomly replaced by a failed one) [33, 49, 83, 85]. For instance, Watts and Newman studied site percolation on small world networks as a model of spreading of disease or information in social networks [83]. It was shown that there exists again a critical fraction of removed nodes above which the network falls apart into a large number of small components. The critical point strongly depends on the topology of the underlying network [83].

3 Chapter

Discrete stochastic model of failure phenomena

To investigate failure phenomena the possibilities of analytical calculations are very limited so that the majority of studies relay on computer simulations using discrete models. This chapter is a brief survey of the most important modeling framework, namely, the fiber bundle model, which was used in my own research.

3.1 Fiber bundle model

One of the major models to study failure of heterogeneous materials is the fiber bundle model (FBM), which was first proposed by Peires in 1927, to test the tensile strength of cotton yarns [87, 88]. Since then several extensions have been introduced [12, 17, 89–91] which made the model more flexible. Today FBM can basically be viewed in two different ways: on the one hand, it is a fundamental model of fibrous materials especially for fibre reinforced composites [17], on the other hand, it can be used as a general modelling framework of systems composed of interacting elements where the local failure of elements triggers failure cascades due to load redistribution. In my research I use FBMs in the second way.

3.1.1 Steps of model construction

The construction of the fibre bundle model is based on the following principles:

Discretization

The basic assumption of FBM is that the examined material is decomposed into a discrete bundle of N number of fibers, placed on a regular lattice (square or triangular), as in Figure 3.1(a). The type of the underlying lattice determines the number of immediate neighbors and hence affects the interaction of fibers. For the sake of simplicity in analytical and numerical calculations, we mostly start from a square lattice.

Failure law

In FBM, it is assumed that fibers are not glued together so the load on the bundle has to be parallel to the direction of fibers. Under an externally increasing load, fibers show completely brittle behaviour, i.e. they deform linearly as by Hooks law

$$\sigma = E\varepsilon \tag{3.1}$$

until a threshold value σ_{th} is reached. Value of young modulus E is same for all fibers. When the fibers are loaded beyond σ_{th}, they suffer immediate failure, i.e. they are removed from the bundle. Failure is irreversible in the sense that failed fibers are never restored.

Distribution of failure thresholds

Heterogeneous materials have a randomness in strength from one component to another. Reasons are grain boundaries, lattice defects, dislocations, vacancies and presence of other impurities. FBM takes this disorder into account by assuming that the strength of fibers (σ_{th}) is a

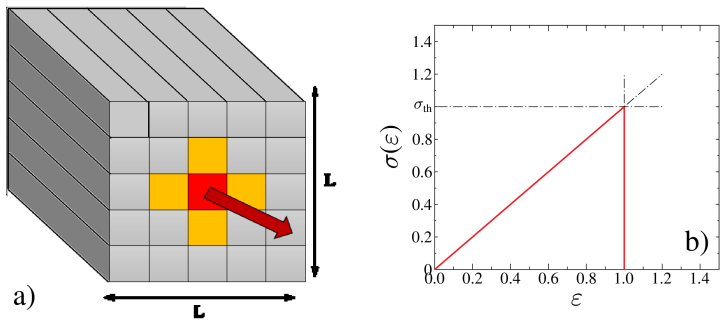

Figure 3.1: (*a*) Set up of the FBM. Parallel fibers are arranged on a square lattice of size $L \times L$, loaded in parallel direction to fibers. When a fiber breaks (red) its load is equally redistributed to the nearest intact neighbours (orange). (*b*) Individual fibers are linearly elastic up to σ_{th}.

stochastic variable characterized by probability density $p(\sigma_{th})$ between (σ_{th}^{min}) and (σ_{th}^{max}) lower and upper limits. The probability distribution $P(\sigma_{th})$

$$P(\sigma_{th}) = \int_{\sigma_{th}^{min}}^{\sigma_{th}^{max}} p(x')dx' \tag{3.2}$$

gives the probability that a randomly selected fiber will break up to a load $\sigma = \sigma_{th}$. Mostly used probability distributions shown in Fig. 3.2 are uniform, exponential and Weibull distributions and their analytical relations are given below respectively.

$$P(\sigma_{th}) = \frac{1}{\sigma_{th}^{max} - \sigma_{th}^{min}} \quad \text{where} \quad \sigma_{th}^{min} \leq \sigma_{th}^{max} \tag{3.3}$$

$$P(\sigma_{th}) = \eta e^{-\eta\sigma_{th}} \qquad \text{where} \quad 0 \leq \sigma_{th} \leq \infty \tag{3.4}$$

$$p(\sigma_{th}) = m\frac{\sigma_{th}^{m-1}}{\lambda^m} e^{-(\sigma_{th}/\lambda)^m} \qquad \text{where} \quad 0 \leq \sigma_{th} \leq \infty \tag{3.5}$$

Whereas, in case of the exponential distribution η is rate parameter which controls the decay of the exponential function. For the Weibull

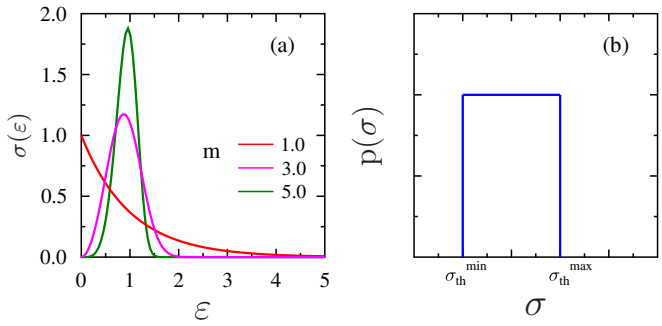

Figure 3.2: Mostly used threshold distributions: (a) Weibull distribution with $\lambda = 1$ for three different values of m. By increasing m the distribution function becomes narrower showing that disorder of the system decreases. (b) Uniform distribution in the interval $[\sigma_{th}^{min}, \sigma_{th}^{max}]$.

distribution the parameters m and λ are shape and scale parameters, respectively. At $m = 1$ the Weibull distribution simplifies to the exponential distribution. Uniform and exponential distribution, because of their feasibility in certain analytical calculations, have primary significance in theoretical studies. The Weibull distribution was introduced in 1939 to describe the randomness of the strength of materials [92, 93]. In our studies we used Weibull distribution and the motivations behind using it are: (i) Behaviour of failure in FBMs with this kind of rapidly decaying strength distribution shows a high degree of robustness that is well understood both in the ELS and LLS limits on $2D$ regular square lattices [94, 95]. (ii) Varying the value of the exponent m in the range $m \geq 1$, the degree of disorder can be controlled in such a way that by increasing m, the width of distribution reduces and as a result the bundle becomes more brittle. This property of distribution is illustrated in Fig. 3.2(a) for different m values. Numerical calculations and experiments have shown already that the degree of disorder has a strong effect on failure of complex systems, this effect can be captured in

FBM by means of threshold distribution $p(\sigma_{th})$.

Load sharing rules

Once a fiber failed, surviving intact fibers have to share its load. The range and form of interaction of fibers is called load sharing rule, which is the most important feature of model and has a strong effect on behaviour of bundle. Mostly two kinds of load sharing rules are considered:
Global load sharing (GLS), also called equal load sharing (ELS), where load is equally distributed among all non-broken fibers regardless of their distance from the broken fiber. ELS appears in real systems if the ends of parallel fibers are perfectly rigidly clamped. In ELS, topology of fibers is irrelevant, no stress fluctuations can arise, and hence, it corresponds to the mean field approximation of FBMs.
Local load sharing (LLS), load of broken fiber is distributed among its local neighbours, generally the nearest neighbors. This happens when at least one end of parallel fibers is not fixed to a rigid support [1, 96, 97]. For simplicity, if we consider the square lattice as shown in Figure 3.1, the number of intact neighbors is 4. When the first fiber breaks, due to the short rang nature of interaction, another fiber can break only in the vicinity of broken fiber. Thus the avalanche of these connected fibers form a cluster that we consider as a crack. As a result of LLS a high stress accumulates near the failed region, i.e. along the edge of crack which strongly affects the propagation of fracture. Fluctuations and spatial correlation can occur in LLS model so the analytical studies based on LLS are not feasible that is a serious limitation of LLS [98–100].

3.1.2 Macroscopic behaviour of FBM

The macroscopic behavior of the fiber bundle can be described by the constitutive curve which can also be determined analytically under ELS conditions. Each fiber has the same elastic constant E but different strengths, randomly selected by a probability distribution. The average

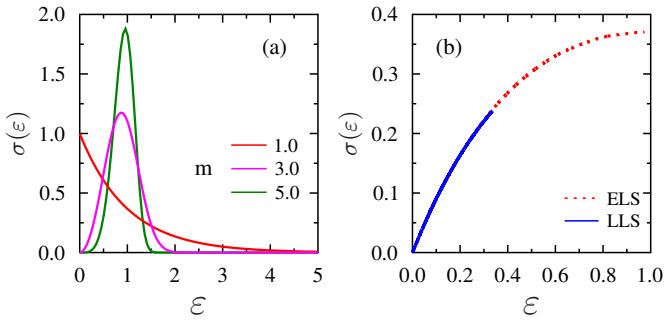

Figure 3.3: (*a*) $\sigma\varepsilon$ curve for an ELS fiber bundle with Weibull distribution at three different exponents m and $\lambda = 1$. By increasing m the distribution becomes narrower, i.e. system becomes more brittle. (*b*) Comparison of the mechanical response of a fiber bundle for ELS and LLS. The stress concentration causes a more brittle behavior of LLS bundles.

number of intact fibers at an extension ε of the bundle is $N(1 - P(E\varepsilon))$ and average force reads as

$$F(\varepsilon) = NE\varepsilon[1 - P(E\varepsilon)], \tag{3.6}$$

since all fibers keep $E\varepsilon$ load. For simplicity, E is usually fixed to 1. As average force per fiber is stress, i.e. $\sigma = F/N$, the mechanical response of the system $\sigma(\varepsilon)$ can be expressed as

$$\sigma(\varepsilon) = \varepsilon[1 - P(E\varepsilon)], \tag{3.7}$$

where $P(x)$ is the cumulative distribution of breaking thresholds [22, 95]. Substituting Eq. (3.5) of the Weibull threshold distribution, the mean field constitutive equation of the bundle is obtained as

$$\sigma(\varepsilon) = \varepsilon e^{-(\frac{\varepsilon}{\lambda})^m}. \tag{3.8}$$

The functional form of Eq. (3.8) is illustrated in Figure 3.3 with different values of m. There are basically two ways to load a specimen, i.e. strain

controlled and stress controlled. In the case of a strain controlled experiment the load required to increase the deformation of the specimen is measured. The specimen is stretched until the first fiber breaks while the deformation is fixed. As a result, a sudden decrease in force equal to the load of broken fiber will occur at this extension. Therefore, no redistribution of the load on intact fibers can occur, hence, in this case fibers break one-by-one as their breaking threshold increases in order. On the other hand, in the stress-controlled case, the load on the specimen is increased slowly and we measure the resulting deformation. In this case when the first fiber breaks, the deformation increases while keeping the load constant. As a result of load redistribution, the local load may exceed the failure threshold of other fibers giving rise to secondary failures without any increment in external load. This breaking step is again followed by load redistribution which may again induced additional failure resulting an avalanche of fiber breaking. This avalanche stops only if intact fibers are strong enough to retain the increased load. When the system becomes stable, the external load is increased again until a catastrophic avalanche occurs when all intact fibers break. In the stress-controlled case the constitutive curve σ of the bundle can only be realized up to the maximum where the specimen suffers a global failure in the form of a catastrophic avalanche. The macroscopic behavior of the bundle is also influenced by the way the load is redistributed. Under stress-controlled loading, in the LLS case the $\sigma\varepsilon$ curve follows the response obtained form ELS but the critical load is lower, i.e. the system is more brittle than in the case of ELS, as shown in figure 3.3(b).

3.1.3 Cracking avalanches in the fiber bundle model

As general description of avalanche dynamics is mentioned earlier in previous chapter. Here are some more details in the framework of FBM. Size of avalanche denoted by Δ is the number of fibers broken between

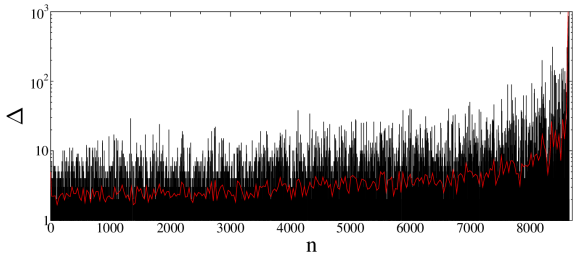

Figure 3.4: Avalanches of a bundle of fibers containing 10^5 fibers as a function of their sequence number. The red line indicates the average avalanche size Δ. It can be observed that the fracture process accelerates as approaching the critical point of the global failure.

two consecutive stable states. In figure 3.4, avalanche sizes of a fiber bundle having 10^5 fibers are shown as a function of their sequence number. It can be observed that the avalanche sizes are fluctuating due to disorder, but on moving towards failure, their average size increases. This behavior indicates that the fracture process accelerates as it approaches the critical point. Size distribution of avalanches can be determined analytically [17].

$$\frac{P(\Delta)}{N} = \frac{\Delta^{\Delta-1}}{\Delta!} \int_0^{\sigma_c} a(\sigma)^{\Delta-1} e^{-a(\sigma)\Delta} [1 - a(\sigma)] p(\sigma) d\sigma, \tag{3.9}$$

where $a(\sigma) = \sigma p(\sigma)/[1 - P(\sigma)]$ gives the number of secondary breakings caused by the breaking of a single fiber at a given load σ. A further analysis of the integral term shows that the asymptotics of the distribution can be described by a power function

$$p(\Delta) \sim \Delta^{-\tau}. \tag{3.10}$$

The value of the exponent τ for ELS is 5/2 which is universal for a broad class of threshold distributions [101], while for LLS it has a significantly higher value, which also depends on the threshold distribution. Figure 3.5

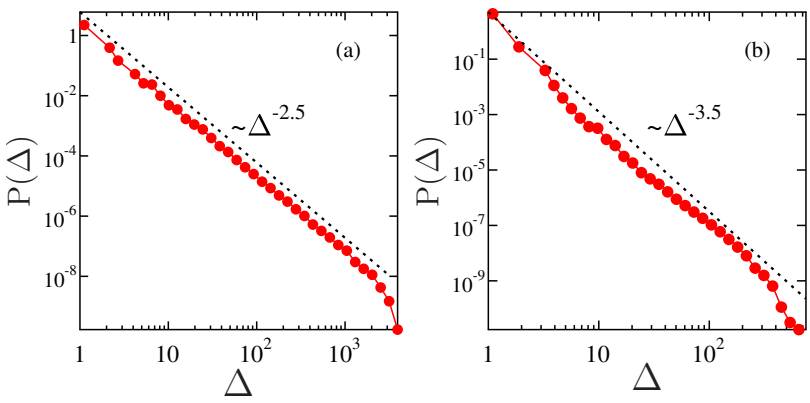

Figure 3.5: The size distribution of avalanches $p(\Delta)$ shows a power law behavior with an exponent of (a) 5/2 for ELS, (b) 7/2 for LLS. The results were obtained by computer simulations of FBMs with $N = 10^6$ fibers.

shows avalanche size distributions for exponentially distributed breaking thresholds both for ELS and LLS. Alex Hansen and his coworkers [17, 89] shown that avalanche size distribution shows a universal power law behavior for any distribution of bundle strength for which the constitutive curve $\sigma(\varepsilon)$ has a single quadratic maximal. If constitutive curve have any inflexion, it still shows power law behaviour but with different exponent values [18]. In the case of LLS, burst size distribution cannot be determined analytically, the above exponent value were determined using computer simulations [89, 101]. Significantly higher exponential value compared to ELS shows that in the presence of stress concentration in the system large avalanches cannot spread stably, because high stress accumulation at a low external load results in a catastrophic failure.

3.1.4 Size dependence of critical strength

The randomness of the breaking thresholds of fibers in FBMs represents the disorder of materials which plays an essential role in fracture processes. FBMs reproduce the so-called statistical size effect of fracture strength, i.e. the fiber bundle model reports that the load carrying capacity $\langle \sigma_c \rangle$ of heterogeneous materials decreases with the number N of fibers. This statistical size effect in the model can be explained by the fact that larger systems are more likely to have weaker fibres, which can trigger a catastrophic avalanche sooner, i.e. under lower external loads. An important characteristic of the size effect for applications is the limit to which the load carrying capacity converges for large systems.
In the case of equal load redistribution, by increasing the number of fibers the critical strength $\langle \sigma_c \rangle$ of the bundle decreases and converges to well defined asymptotic values $\sigma_c(\infty)$, as shown in Figure 3.6(a). This convergence can be described analytically by a power law functional form

$$\langle \sigma_c \rangle = \sigma_c(\infty) + AN^{-\alpha}, \tag{3.11}$$

where $\sigma_c(\infty)$ denotes the asymptotic bundle strength. The scaling exponent α has the value $\alpha = 2/3$ is universal for a wide class of breaking thresholds, while the multiplication factor A depends on the shape of the threshold distribution [17]. The critical strength of an infinite system $\sigma_c(\infty)$ is the maximum of the constitutive curve Eq. (3.7). Figure 3.6(b) shows that Eq. (3.11) is in agreement with the simulation results of ELS bundles. In the figure, the value of $\sigma_c(\infty)$ was considered a free parameter, which we keep tuning until the best straight line was obtained on a double logarithmic plot. However, in the local load redistribution case, we obtain an entirely different size dependence. Both numerical and analytical calculations revealed a logarithmic decrease [18]

$$\langle \sigma_c \rangle \approx \frac{1}{[\ln N]^{\beta}}. \tag{3.12}$$

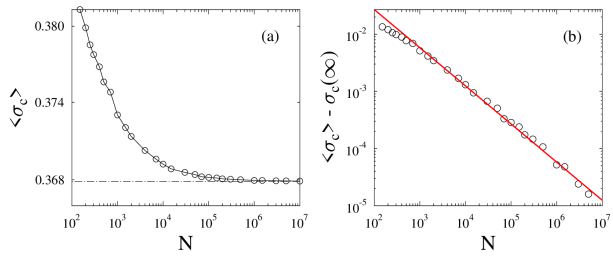

Figure 3.6: System size dependence of the average strength of ELS fiber bundles with exponentially distributed breaking thresholds.

where the exponent β was found to depend on the precise range of load sharing.

4 Chapter

Objectives

In the framework of my PhD I carried out research in two main directions: First, I tried to obtain a deeper understanding of the phase transition analogy of fracture processes. For this purpose I studied how a solid body perforates due to dynamic impact loading as the energy of impact is varied at different amounts of materials' disorder. I worked out a simple model of a bar shaped specimen subject to three-point bending by impact in the middle. I wanted to clarify how the system approaches the critical point of perforation, i.e. the point where the bar breaks through. My goal was to identify the order parameter of the damage to perforation transition and to determine the value of the critical exponents characterizing the system in the vicinity of the critical point. It was also a crucial question how robust the behaviour of the system is against the degree of disorder.
As to the next, my research focused on the cascading failure mechanism of complex systems initiated by external load increments. The emergence of crackling avalanches in heterogeneous solids under an external load and the spreading of failure cascades e.g. in technological networks share several common features, i.e. they are both driven by the redistribution of load after local damage events, and the stochastic strength of the elements of the system plays a crucial role in avalanche propagation. I

investigated the local failure mechanism of heterogeneous materials on complex networks with the goal to understand how the interplay of the topology of the network of load transmitting connections and the disordered local strength affects the statistical and dynamical features of failure cascades.

In both studies I used the fiber bundle model (FBM) of heterogeneous materials due to its flexibility to capture the disordered strength of elements and the mechanism of load transmission from failed to intact elements of the system. In case of impact fracture, the bar shape specimen was composed of two rigid blocks which were glued together by an elastic interface. I constructed an FBM to discretize the interface where cracking was induced by impact. The rigidity of the two blocks ensured global (but not equal) load sharing over the intact fibers of the interface, which made it possible to perform analytical calculations up to some extent.

To generate complex networks with controllable structural features I used the WS model. Starting from a square lattice of fibers the network of load transmitting connections was gradually randomized. I applied localized load sharing to redistribute the load after fiber breakings, and used computer simulations to reveal how failure cascades change when the structure of the network is tuned from completely regular to completely random. Most notably, I showed that as the network topology changes a transition emerges from the localized to the mean field behaviour of FBMs. It was my goal to understand the mechanism of this transition and to clarify how the degree of strength disorder of fibers affects the transition.

Failure avalanches gradually spread on the interaction network through consecutive steps of local failure and load redistribution. Analyzing the temporal evolution of failure avalanches I wanted to give a detailed description of the relation of the temporal profile of avalanches and the structure of the underlying network.

5 Chapter

Impact induced transition from damage to perforation

I studied the impact induced failure of a bar shaped sample of heterogeneous materials using a three point bending model, while focusing on how system undergoes perforation when gradually increasing the impact energy. The main goal of this study was to obtain a better understanding of the damage to perforation transition, in particular, its analogies to continuous phase transitions. I performed numerical calculations to calculate the critical exponents of phase transition and derived scaling relations in terms of the number of fibers and degree of disorder. This work is published in Ref. [23]

5.1 Stochastic interface model

We used a three-point bending arrangement of a bar shaped sample to study the damage to perforation transition in an impact loading process. The sample consists of two rigid blocks of lengths a and b which are glued together with the help of an elastic interface of width $l_0 \ll b$. Ends of the sample are clamped by fixing outer upper corners of blocks to a support around which they can undergo a rigid rotation. Source of external load

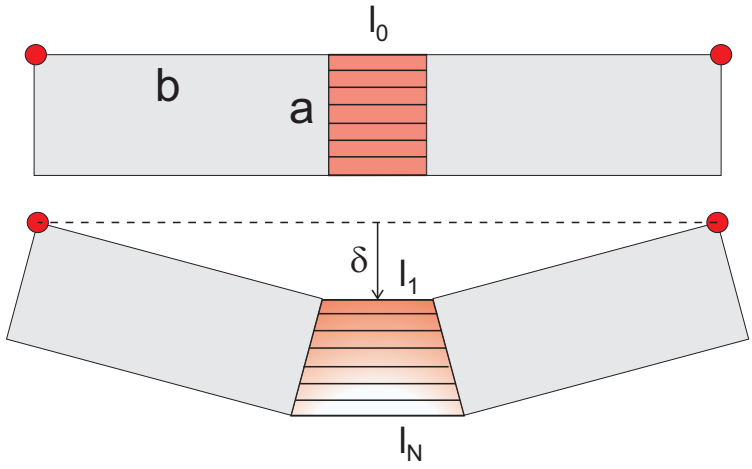

Figure 5.1: Three point bending model of sample which consists of two rigid blocks of lengths a and b glued together by an elastic interface. The deflection δ of middle point of bar characterizes its deformation under the effect of impact. Due to impact loading a linear deformation profile is built up along the interface where top fibers have smallest l_1 and bottom fibers have largest l_N lengths.

is an impactor with a downward velocity that hits bar in middle as illustrated in Fig. 5.1. As a result, the bar deflects and the interface between blocks accommodates the whole deformation. To understand how bar fractures, we discretized the interface by a bundle of N number of parallel breakable fibers having length l_0 and stochastic strength, equidistantly placed between blocks. When the bar undergoes deflection, fibers can only suffer stretching as they have no bending rigidity. $\varepsilon_c^i, i = 1, \ldots, N$ is the threshold deformation, up to which fibers are supposed to show linearly elastic behavior and above which they undergo irreversible failure. Young modulus Y is supposed to be identical for each fiber, hence, the material's disorder is represented solely by the random breaking thresholds sampled from probability density function $p(\varepsilon_c)$. As

the blocks are clamped, deformation of the sample can be characterized by only one variable δ that is the deflection of middle point of bar. Fig. 5.1 illustrates the loading condition and geometrical setup of the model. At a finite deflection $\delta > 0$, fibers endure elongation Δl increasing from top to bottom causing an opening in interface. From the geometrical arrangement of Fig. 5.1, the length of fibers l_i can be written as

$$l_i = l_1 + 2\delta \frac{a}{b} \frac{i-1}{N-1}, \qquad i = 1, \ldots, N \tag{5.1}$$

here index i points out the fiber's position starting from top of interface. Length of the first fiber is $l_1 = l_0 + 2(b - \sqrt{b^2 - \delta^2})$. Hence, the local elongation $\Delta l_i = l_i - l_0$ of fibers can be expressed as

$$\Delta l_i = 2b - 2\sqrt{b^2 - \delta^2} + 2\delta \frac{a}{b} \frac{i-1}{N-1}, \tag{5.2}$$

which gives a linear deformation profile $\varepsilon_i = \Delta l_i / l_0$ through the interface. Fracture is started when an impactor of mass m hits in the middle of bar with initial velocity v_0. For simplicity, we suppose that the specimen's mass is negligible in comparison to impactor, moreover, during whole fracture process, bar and impactor remain in contact. However, the initially imparted kinetic energy $E_0 = 1/2mv_0^2$ will be partly converted to elastic energy E_{el} of stretched fibers and partly dissipated E_{dis} by breaking fibers. The energy balance of this process can be expressed as

$$E_0 = E_k(\delta(t)) + E_{el}(\delta(t)) + E_{dis}(\delta(t)), \tag{5.3}$$

at any time t as the system expands. In Eq. (5.3), first term E_k on right hand side represent the impactor's kinetic energy

$$E_k = \frac{1}{2} m v^2 \tag{5.4}$$

where v is the velocity of impactor, i.e. the derivative of deflection of specimen $v = d\delta/dt$. Fibers slowly get deformed due to increasing deflection and ultimately break when the local breaking threshold is

exceeded. Elastic energy E_{el} stored by elongation of a single fiber Δl can be expressed as $E_{el} = \left(\frac{ac}{2Nl_0}\right) Y \Delta l^2$, where ac/N is the cross sectional area assigned to the fiber where the specimen is assumed to be of unit thickness i.e. $c = 1$. However, at deflection δ, the analytical expression for E_{el} stored in the deformation of whole interface, in terms of fiber's disorder distribution can be written as

$$E_{el}(\delta) = \frac{ac}{2Nl_0} Y \sum_{i=1}^{N} \left[1 - P(\varepsilon_i(\delta))\right] \Delta l_i(\delta)^2. \tag{5.5}$$

$P(x)$ here is the cumulative distribution of breaking thresholds, whereas, the term $[1 - P(\varepsilon_i(\delta))]$ gives the probability that at deflection δ, the i_{th} fiber along the interface is intact. The expression for dissipated energy E_{dis} is given as

$$E_{dis} = \frac{ac}{2Nl_0} Y \sum_{i=1}^{N} \int_0^{\Delta l_i(\delta)} p(x) x^2 dx, \tag{5.6}$$

considering that E_{el} accumulated in a fiber at the time when it breaks is utilized to create the corresponding crack surface.
To analyze the effect of materials' degree of disorder on the transition from damage to perforation, we used uniform distribution for sampling the breaking thresholds, of the form

$$p(\varepsilon_c) = 1/(2W) \quad \text{for} \quad \varepsilon_c^0 - W \leq \varepsilon_c \leq \varepsilon_c^0 + W, \tag{5.7}$$

where ε_c^0 is the average fiber strength. We have fixed the value of ε_c^0 for all calculations, however, the width of the distribution W is the only parameter that controls the degree disorder of the system. In the calculations W was varied in the range $0 \leq W \leq \varepsilon_c^0$. Fig. 5.2($a$) illustrates the disorder distribution $p(\varepsilon_c)$ for different values of W. When impactor hits the bar, a linear deformation profile sets up along the interface as a result of induced deflection, as stated by Eq. (5.2). At $W = 0$ there is no disorder, sample have same breaking thresholds

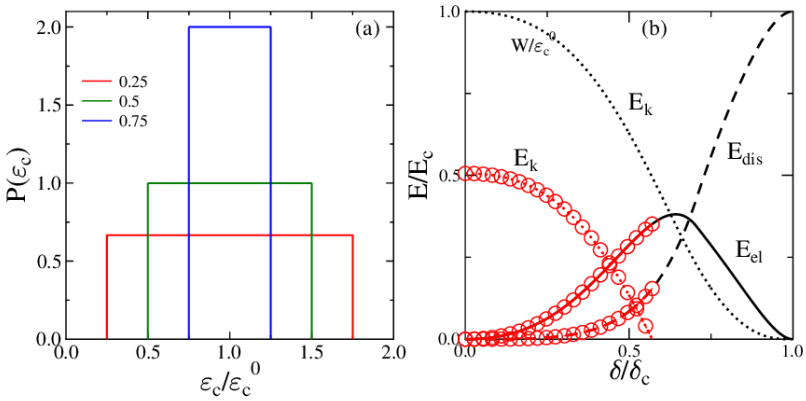

Figure 5.2: (a) Probability distribution $p(\varepsilon_c)$ of breaking thresholds at three different values of width $W/\varepsilon_c^0 = 0.25, 0.5, 0.75$. (b) The energy evolution during impact process at critical impact energy $E_0 = E_c$. Red symbols represent the case of a sub-critical impact at $E_0 \approx E_c/2$.

$\varepsilon_c^i = \varepsilon_c^0$ $(i = 1, \ldots, N)$, hence, the fiber at position $(i = N)$ i.e. at the bottom of interface, breaks first. Consequently, a crack emerges, which advances in upward direction and stops when the last fiber at position $(i = 1)$ breaks. On the other hand, at $W > 0$ when the system has a finite disorder, the order of breaking is determined both by the strain ε_i and local strength ε_c^i, hence, we get a random breaking sequence of fibers through the interface. The value of the deflection δ_c^i at which individual fibers break can be determined by inverting Eq. (5.2)

$$\delta_c^i = \delta(i, \varepsilon_c^i), \qquad i = 1, \ldots, N. \tag{5.8}$$

So the deflection thresholds δ_c^i depend upon two independent variables, i.e. the strength ε_c^i and position i of the fiber. During the gradual deflection of bar, fibers start breaking in increasing order of deflection thresholds δ_c^i, $(i = 1, \ldots, N)$ which results a random sequence of breaking events along the interface in linear deformation profile. Computer simulations of this impact process is carried out in following steps: at the

initial stage random threshold values ε_c^i (i=1,..., N) are given to each fiber using the distribution Eq. (5.7). Deflection thresholds δ_c^i are obtained from Eq. (5.8) and then sorted in ascending order. Elastic E_{el} and dissipated E_{dis} energies are determined using Eqs. (5.5,5.6) as function of δ. Simulations were performed to investigate the transition from damage to perforation and to analyze the effect of disorder, for different number of fibers in the range varying between $N = 10^3$ and 10^7, at different values of disorder parameter $W/\varepsilon_c^0 \in [0, 1]$. Geometrical layout of sample was fixed to $b/a = 2.5$, $l_0/a = 0.02$ and $a = 1$.

5.2 Energetics of loading process

As stated earlier, the bar undergoes deflection when impactor hits it with initial kinetic energy E_0, and interface fibers start breaking. At low imparted energy the interface only suffers partial breakdown and keeps the integrity of the specimen because the damage process stops at certain maximum deflection δ_m. At stopping point, sum of dissipated and elastic energies must to be equal to initial impact energy E_0

$$E_0 = E_{el}(\delta_m) + E_{dis}(\delta_m). \tag{5.9}$$

Putting Eqs. (5.5 and 5.6) into Eq. (5.9) we can estimate E_0 which is required to achieve a maximum deflection δ_m. When E_0 is sufficiently high, the damage process does not stop and the specimen perforates as all fibers get broken. First it occurs at critical input energy E_c, at which deflection stops when the last fiber breaks with the greatest critical deflection δ_c^i, defining the system's critical deflection δ_c. It came out that critical energy E_c is equal to the total dissipated energy $E_{dis}(\delta_c)$ that is required to break the entire interface.
The elastic energy $E_{el}(\delta)$, dissipated energy $E_{dis}(\delta)$, and remaining kinetic energy $E_k(\delta)$ of impactor are shown in Fig. 5.2(b) as function of deflection δ of the sample at critical energy $E_0 = E_c$ for a system with

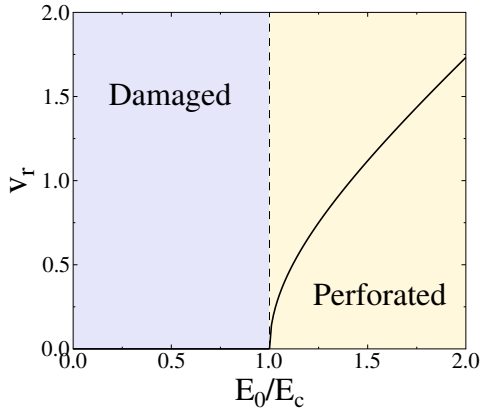

Figure 5.3: v_r the remaining velocity of impactor as a function of impact energy E_0. In the damage phase $v_r = 0$ as the impactor stops at a partial failure of specimen, whereas beyond the perforation limit $E_0 > E_c$ impactor keeps moving with a certain value of v_r after the specimen breaks into two pieces. Impactor is supposed to have a unit mass.

$N = 10^6$ fibers at highest disorder $W/\varepsilon_0^c = 1$. The remaining kinetic energy of the impactor $E_k(\delta)$ was calculated as

$$E_k(\delta) = E_0 - [E_{el}(\delta) + E_{dis}(\delta)]\,, \tag{5.10}$$

where E_0 is determined from Eq. (5.9) at $\delta_m = \delta_c$. As in the example the disorder distribution goes down to zero strength value, breaking already starts at very low deflection. Fig. 5.2(b) shows that the dissipated energy E_{dis} increases monotonically, whereas elastic energy E_{el} has a maximum at a distinct deflection value. Where a monotonically decreasing behaviour of remaining kinetic energy E_k can be observed which goes to zero at critical deflection. Figure also shows the energetics of a sub-critical impact $E_0 \approx E_c/2$ at which the bar gets damaged because of fiber breaking, but not perforates. Since E_{el} and E_{dis} are completely determined by bar's deflection δ, so these curves coincide with their critical energy counterparts obtained at $E_0 = E_c$. However, at maximum

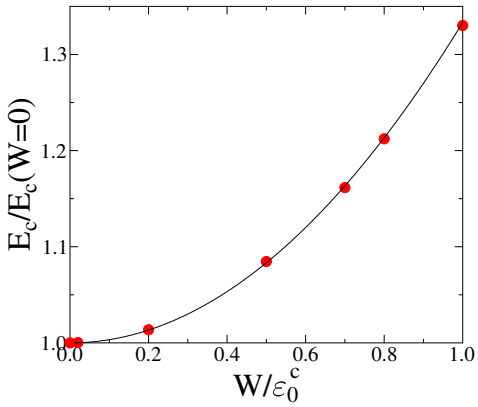

Figure 5.4: The critical energy E_c of perforation as a function of degree of disorder W/ε_0^c. Solid line represents the analytical solution Eq. (5.12), whereas symbols represent numerical measurements. E_c is divided by its zero disorder counterpart.

deflection δ_m, i.e. at the end of red curves, kinetic energy E_k is zero as the impactor stops. The specimen perforates in super-critical phase $E_0/E_c > 1$ so that the impactor continues its motion. The E_{el} and E_{dis} curves still coincide with corresponding curves obtained at critical point $E_0/E_c = 1$, however, kinetic energy E_k does not drop to zero. Rather, the impactor keeps moving with remaining energy E_k obtained at the critical deflection δ_c. Fig. 5.3 illustrated this super-critical phase by the ballistic diagram, where the impactor's remaining velocity v_r is plotted as a function of the applied energy. Value of v_r was calculated as

$$v_r = \sqrt{\frac{2}{m}\,(E_0 - E_c)}, \qquad \text{for} \qquad E_0 \geq E_c. \tag{5.11}$$

Fig. 5.3 highlights the two phases of impact process: The damaged phase at $E_0 < E_c$, the $v_r = 0$ because impactor stops at maximum deflection δ_m, whereas in perforated phase there is a finite value of remaining velocity $v_r > 0$, as impactor keeps a fraction of initial energy after breaking the interface.

5.3 Effect of the finite number of fibers and disorder on the critical point

It is important to know how the impact induced failure of the specimens is affected by the amount of material's disorder. Starting from the disorder distribution Eq. (5.7) and using the dissipated energy Eq. (5.6) one can easily derive the expression of the critical energy E_c in terms of the parameters of the system. As the dissipated energy of a single broken fiber depends exclusively on its breaking threshold ε_c, the integral of Eq. (5.6) can be simplified to integrating over the range of threshold values. However, the disorder dependence of critical energy E_c can be expressed in the form

$$E_c = \frac{ac}{12Wl_0}[(\varepsilon_0^c + W)^3 - (\varepsilon_0^c - W)^3]. \tag{5.12}$$

It can be seen that E_c increases monotonically from
$E_c(W = 0) = (ac/2l_0)(\varepsilon_c^0)^2$ at zero disorder to
$E_c(W = \varepsilon_c^0) = (2ac/3l_0)(\varepsilon_c^0)^2$ at the maximum disorder. Fig. 5.4 shows that the numerical measurements are in good agreement with analytical expression of critical energy given in Eq. (5.12).
As critical energy E_c is an integrated quantity of whole sample it has very small fluctuations when it is calculated for a single sample by using a finite number N of fibers. Whereas, deflection values at which the bar starts damaging δ_d and ultimately perforates at δ_c, strongly depend on both degree of disorder W and number of fibers N. To quantify these dependencies, I performed numerical simulations of impact process by varying N from 10^3 to 10^7 at several values of W. Deflection values of a single sample at which breaking of the first and the last fiber occurs are named as damage threshold δ_d and critical deflection δ_c, respectively. I then averaged these values over 1000 samples for each parameter set. It is clear from Fig. 5.5(a, b) that the critical deflection δ_c and the damage threshold δ_d both depend on N which we use to discretize the interface. However, δ_d decreases, whereas δ_c increases and both converge to

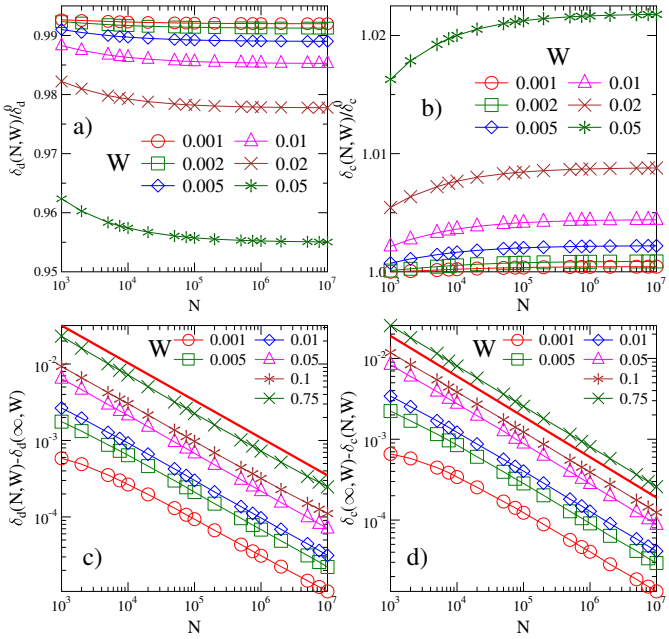

Figure 5.5: Effect of number of fibers N and degree of disorder W on damage threshold δ_d and on critical deflection δ_c of system.

well-defined asymptotic values $\delta_d(\infty, W)$ and $\delta_c(\infty, W)$ in the limit $N \to \infty$. Both quantities are normalized by their counterparts at zero disorder

$$\delta_d^0 = a\left[\sqrt{1+\frac{bl_0\varepsilon_c^0}{a^2}}-1\right], \tag{5.13}$$

$$\delta_c^0 = \frac{l_0\varepsilon_c^0}{2}\sqrt{\frac{4b}{l_0\varepsilon_c^0}-1}, \tag{5.14}$$

which are independent of N. It is observed that as the disorder W increases, the asymptotic values $\delta_c(\infty, W)$ and $\delta_d(\infty, W)$ deviate more

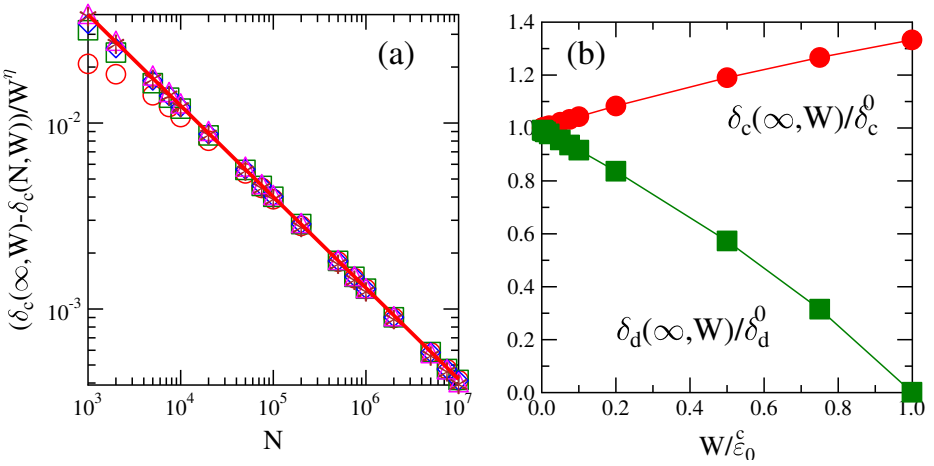

Figure 5.6: (a) Rescaling transformation of the δ_c curves of Fig. 5.5(d) with a power of W. (b) The asymptotic values of critical deflection and damage threshold as function of W.

and more from their zero disorder values. Figures 5.5(c,d) indicate that the convergence of $\delta_c(N,W)$ and $\delta_d(N,W)$ to their corresponding asymptotic values exhibits interesting universal features, that is at any value of $W>0$ the distances $\delta_c(\infty,W)-\delta_c(N,W)$ and $\delta_d(N,W)-\delta_d(\infty,W)$ drop to zero as a universal power law of N. In the figures, solid straight lines are for power laws with exponent $-1/2$. Value of this exponent is independent of amount of disorder, but, a shift of the curves is observed with respect to each other at increasing W. It is demonstrates in figure 5.6(a), that by rescaling δ_c with a suitable power η of W, the curves obtained at different disorders fall on the top of each other. Same systematic is valid for δ_d. Based on this numerical analysis, the N and W dependence of critical and damage threshold deflection can

be cast into the following scaling forms

$$\delta_d(N,W) = \delta_d(\infty,W) + AW^{\eta}N^{-\mu}, \quad (5.15)$$

$$\delta_c(N,W) = \delta_c(\infty,W) - BW^{\eta}N^{-\mu}, \quad (5.16)$$

where scaling exponents μ and η both have $1/2$ value. Eqs. (5.15,5.16) show that the asymptotic values of both perforation and damage thresholds are disorder dependent. The asymptotic values $\delta_d(\infty,W)$ and $\delta_c(\infty,W)$ were obtained by fine tuning to get the best straight lines shown in Figs. 5.5(c,d) on a double logarithmic plot. Final result is presented in Fig. 5.6(b), where asymptotic values of both damage and critical deflection are normalized by their respective zero disorder counterparts given in Eqs. (5.13,5.14). It is clear form the figure that for increasing disorder the interface starts damaging earlier, whereas perforation occurs at higher value of deflection if sufficient input energy is applied to the system. An important finding of analysis is that for a reasonably fine discretization, results are independent of number of fibers. In next study of perforation transition I fixed the number of fibers of discretization to $N = 10^6$.

5.4 Approaching the critical point

To fully understand how the system is approaching to the critical point of perforation, numerical simulations were performed by varying the imparted energy E_0 below E_c for many values of disorder W. Fig. 5.7(a) shows the maximum deflection δ_m of impact process as a function of input energy E_0. It can be seen that δ_m increases monotonically with E_0 to a critical deformation $\delta_c = \delta_m$ achieved at $E_0 = E_c$. The deflection rate $\delta'_m = d\delta_m/dE_0$ however, is not monotonous, i.e. starting from a rather high value δ'_m first it decreases at low energies to a finite minimum and then it grows and seems to diverge while approaching to critical energy.

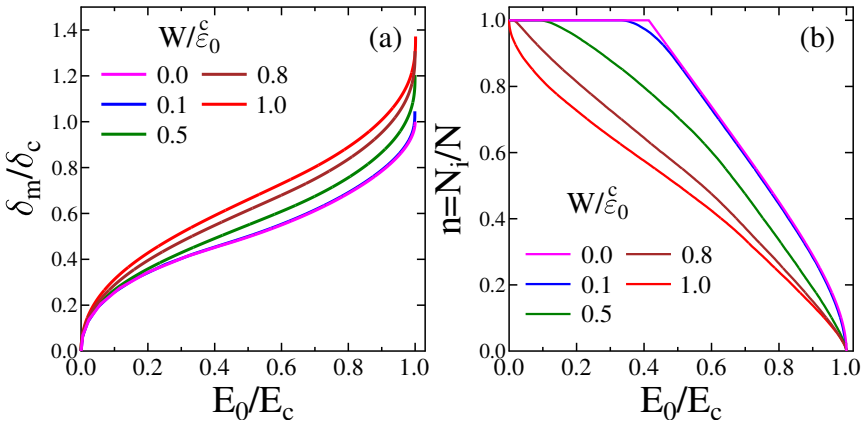

Figure 5.7: (a) Maximum deflection of a bar δ_m as a function of input energy E_0 for different disorder strengths W. (b) Fraction of remaining fibers $n = N_i/N$ as a function of input energy E_0 for different values of W.

As the impact energy is gradually increased, the interface gets more and more damaged leading to a growing final state deformation. Bar's damage state is characterized by the fraction of intact fibers $n = N_i/N$, N_i wher represents the number of intact fibers when the maximum deflection reached at an initial energy E_0. It is shown in Fig. 5.7(b) that n decreases monotonically as a function of E_0 starting from 1 and converging to 0, when the critical point of perforation E_c is reached. Note that at low disorders, the $n(E)$ curves initially have a constant regime $n = 1$, as the final stage deflection has to exceed the damage threshold $\delta_m > \delta_d$ to start breaking the fibers. Figure also illustrates that at a certain fraction of critical energy E_0/E_c the fraction of load bearing intact fibers n of the specimen is lower indicating a higher damage $d = 1 - n$ at higher disorder W. For better understanding of transition from damage to perforation, I analyzed the behaviour of system in the vicinity of critical point E_c. As stated earlier, with increasing input

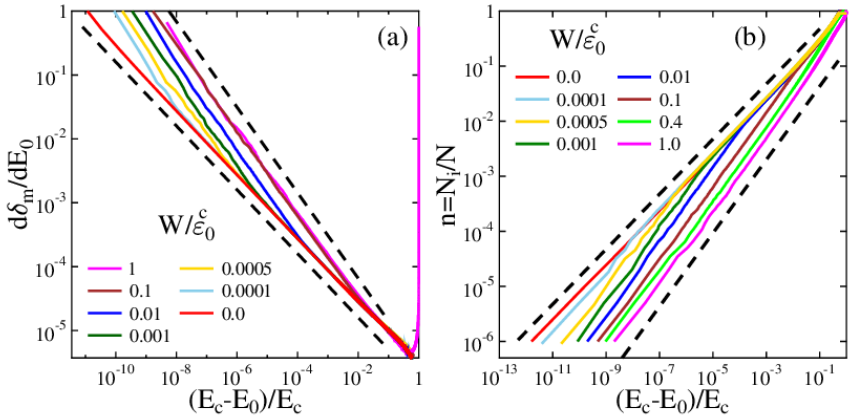

Figure 5.8: (a) Derivative of the maximum deflection δ_m with respect to the imparted energy E_0 as a function of the relative distance from the critical point $(E_c - E_0)/E_c$ for different values of disorder W. (b) Fraction of remaining fibers as a function of distance from the critical point $\Delta = (E_c - E_0)/E_c$ for several values of W.

energy the critical point of perforation is approached with an acceleration of the deformation of the bar so that δ'_m diverges in the $E_0 \to E_c$ limit. It implies that close to E_c, the system gets more susceptible to little increments of the imparted energy responding with a fast growing deflection. To quantify this susceptibility, I determined the rate of deflection δ'_m by numerical differentiation of the $\delta_m(E_0)$ curves for different values of disorder strength W.
Figure 5.8(a) shows that for $W = 0$ the rate of deflection diverges as a power law of distance from critical point.

$$\delta'_m \sim (E_c - E_0)^{-\gamma}, \tag{5.17}$$

where value of exponent γ is $1/2$. Note that for a system with size $N = 10^6$ an excellent quality of power law over 8 orders of magnitude is

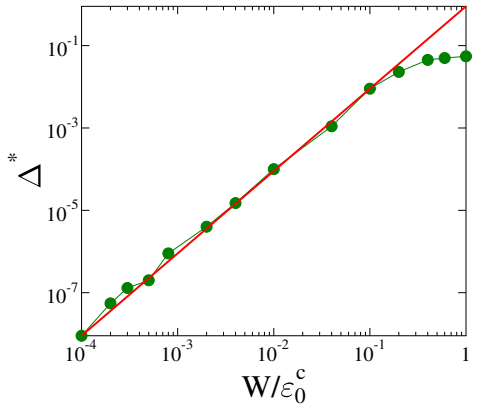

Figure 5.9: The crossover point Δ^* as a function of disorder W/ε_0^c. The straight line is a power law of exponent 2.0.

obtained. It is very important to highlight that at non-zero disorder $W > 0$, i.e. when fibers have a random breaking thresholds, the power law divergence retains, however, a crossover appears between two regimes of different exponents: away from E_c the exponent of power law coincides with its counterpart at zero disorder $\gamma = 1/2$, whereas closer to the critical point a higher exponent $\gamma = 2/3$ is obtained due to the acceleration of deflection.
The emergence of this scaling behaviour near the critical point is also supported by the behavior of the intact fibers n. Fig. 5.8(b) shows that re-plotting n as a function of $E_c - E_0$, a good quality power law is obtained for zero strength disorder

$$n \sim (E_c - E_0)^{\beta}, \tag{5.18}$$

where the exponent has the value $\beta = 1/2$. The fraction of surviving fibers n is always zero in the perforation phase $E_0 > E_c$, while in the partial failure phase it has a non zero value $n > 0$ that tends to zero as a power law of distance from the critical point while approaching E_c. Because of this behavior of n we can consider it as the order parameter

and β is the exponent of order parameter of the damage to perforation transition. At a finite value of disorder $W > 0$, same qualitative behavior is observed for deflection rate too, i.e. the power law functional form holds, however, again a crossover occurs between two regimes of different exponents. Close to perforation n goes to zero with a high value of exponent $\beta = 2/3$, however, away from critical point, exponent has its zero disorder value $\beta = 1/2$ (see Fig. 5.8(b)). Comparison of Figs. 5.8(a),5.8(b) reveals the disorder dependence of position of crossover point Δ^*: At higher disorder, the crossover where exponents β and γ shift to their larger value, appears earlier at a larger distance from critical point. Using the data of Fig. 5.8(a), I determined the crossover point Δ^* as the intersection point of two fitted power laws of exponents 1/2 and 2/3. Fig. 5.9 presents Δ^* as a function of W. It is clear that Δ^* goes to zero in zero disorder limit since curves of δ'_m and n are described by a single exponent of value 1/2. As the disorder W increases, the value of Δ^* grows rapidly and becomes steady above $W/\varepsilon_0^c \approx 0.15$. Figure also shows that the increasing part of the $\Delta^*(W)$ curve can be approximated by a power law

$$\Delta^* \sim W^{\xi}, \tag{5.19}$$

here exponent was obtained numerically as $\xi = 2.0 \pm 0.05$. By saturation of crossover point Δ^*, it means that beyond a definite value of W any further increment of disorder has no relevant effect. To understand this behaviour, the geometric structure of damage need to be analyzed. At $W = 0$, the perforation appears in this way that a crack initiates at bottom of interface and moves upwards when impactor moves forward. However, at $W > 0$ fibers have random breaking order along the interface. Strain gradient given by Eq. (5.2) and the strength disorder Eq. (5.7) of fibers give rise to a complex damage profile along the interface: at a certain deflection δ the breaking probability of bottom fibers of interface is high and form a crack, while fibers at the top have high chance to be intact. Hence there are two regimes which can be separated

by a random sequence of intact and broken fibers that act as a process zone in front of crack tip. When W increases the process zone becomes wider, and for fairly large W it can stretch over entire interface. This case of strong disorder happens if at the deformation where the top of the interface may suffer damage $\varepsilon_1(\delta) > \varepsilon_0^c - W$, the bottom of interface may be still intact $\varepsilon_N(\delta) < \varepsilon_0^c + W$. Here ε_1 and ε_N are fiber's strains at the top and bottom of the bar. Using Eqs. (5.2,5.7) and considering that $b \gg \varepsilon_0^c + W$ the condition for strong disorder can be expressed as

$$W^* \approx \frac{a^2}{2b}\left[\sqrt{1+\frac{4b\varepsilon_0^c}{a^2}}-1\right]. \tag{5.20}$$

It can be seen that for $W > W^*$, the disorder is high enough so that there is no crack formation, damage can happen anywhere alongside interface, though the probability of fiber breaking is higher closer to the bottom. These results imply that the significance of disorder in the interface damaging is determined all together by the geometrical setup of the specimen a, b, by the average ε_0^c and by the width W of the strength distribution. The crossover point Δ^* has W dependence only in the weak disorder regime $W < W^*$. The $W^* \approx 0.22$ obtained from Eq. (5.20) is in a good agreement with the numerical findings.

5.5 Conclusions

I studied the failure of a bar shaped sample induced by an impactor, to understand how perforation occurs when the impact energy is slowly increased. Based on numerical and analytical calculations in a simple three-point bending model of a bar, I showed that the result of the impact process can be divided into two states based on the input energy E_0: at low E_0, the bar only undergoes a finite deflection and fails partially. However, beyond a critical energy E_c a global failure occurs, i.e. as a result of impact the sample perforates and breaks into two

pieces. To understand how the damage to perforation transition occurs at critical energy E_c, I analyzed the behavior of the deflection rate and of the intact cross section of the bar while it approaches critical point of perforation. Numerical analysis proved that the deflection rate diverges, whereas the fraction of intact fibers tends to zero as a power laws of distance from critical point similar to continuous phase transitions. Power law behavior prevails for any value of disorder W with universal exponents, however, at a definite disorder a crossover occurs between two regimes of different exponents: away from critical point the critical exponents are in good agreement with their counterparts at zero disorder, whereas in the vicinity of critical point both quantities are characterized by higher exponent. Crossover point shows a power law dependence on disorder in weak disorder range, while it is almost constant for highly disordered samples. Various kinds of systems [14, 79, 81, 94, 102–104] have been used to study the disorder dependence of the nature of transition from partial to complete failure. These studies have shown that below a certain value of disorder, fracture becomes abrupt, hence, to get a power law scaling the degree of disorder need to be greater than a threshold value. Contrarily, our system has a unique feature. In our case the transition from damage to perforation shows analogies to continuous phase transitions even in the limit of zero disorder, which can be characterized by critical power laws. Reason behind this important contradiction is the loading condition. In our system the loading condition ensures that fiber's stress and strain is homogeneous which linearly increase with the distance from the position of impact. In addition, the advancing impactor induces a strain controlled loading meaning that the impact position determines the load but in this way that fiber breaking slowly releases the load on the sample. This releasing effect of fibers together with the strain gradient in the sample makes the damage process stable even in the zero disorder limit. For phase transition character of transition from damage to perforation, the

essential role is played by system's global response, guarantied by two rigid blocks of bar. The major simplification of model is that it does not account for stress concentration that arises at the tip of propagating crack in real materials. However, the model calculations suggest that the transition should also occur in the presence of enhanced stress due to overall bending of bar.

6 Chapter

Localized to mean field transition of cascading failures

I investigated failure process of fiber bundles on complex networks with an aim to understand how the network topology of load transmitting connections together with strength disorder of elements affects the cascading failure activity. I used fiber bundle model (see Chapter 3) applying the Watts-Strogatz rewiring technique to obtain a complex network of fibers starting from a square lattice. Here I step-by-step present the main outcomes of my study both for the macro- and microscopic behaviour of the bundle. Details of this work are given in Ref. [28].

6.1 Fiber bundle model on complex networks

To analyze cascading failures I considered a parallel fiber's bundle assuming them to be the nodes of a complex network. A gradually increasing external load is applied parallel to the direction of fibers. To link the model to material's mechanics, we suppose that fibers show linearly elastic behaviour up to threshold load σ_{th}, at which irreversible breaking occurs. Fibers have a fixed Young modulus $E = 1$, however,

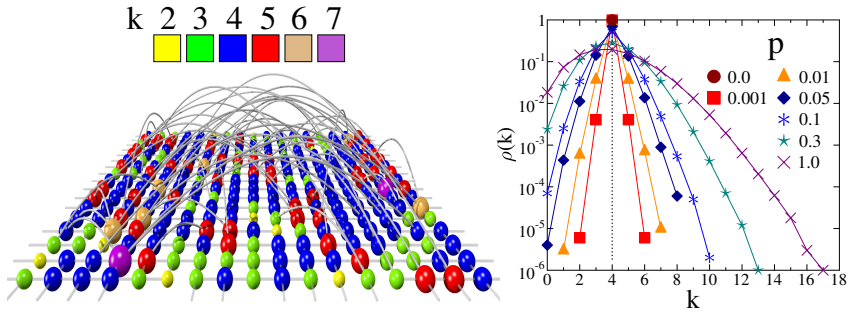

Figure 6.1: Demonstration of model construction. $(left)$ A small lattice of size $l = 17$ is rewired at $p = 0.1$. Spheres denote networks' nodes, colored according to their degree k. For clear understanding of network structure sphere sizes are proportional to node degree and rewired links run outside the plane of the original lattice. $(right)$ The degree distribution $\rho(k)$ of rewired lattices of size $l = 1000$ at different rewiring probabilities p.

fibers have random local strength σ_{th} chosen from a probability density function $p(\sigma_{th})$. Load of a failed fiber is overtaken by surviving unbroken fibers. I applied localized load sharing (LLS), where load redistribution happens along the links of elementary load transmission network.
To obtain a simple network along which load redistribution over fibers takes place, we started from a $2D$ square lattice of length l and $N = l^2$ number of fibers, then Watts-Strogatz rewiring method was applied for randomizing the connections [105, 106]. Fibers are allotted to nodes, perpendicular to plane of original lattice. On a square lattice having periodic boundary conditions in both directions, all fibers have four nearest neighbors, so, degree distribution $\rho(k)$ has simple initial form

$$\rho(k) = \begin{cases} 1 & \text{for} \quad k = 4, \\ 0 & \text{otherwise.} \end{cases} \tag{6.1}$$

In next step, each of initially existing $L = 2N$ links are rewired with a probability p $(0 \leq p \leq 1)$. A new fiber is assigned randomly to both ends

of rewired link from the bundle under the condition that no multiple links or loops are allowed between fibers (see Fig. 6.1($left$)). Hence rewiring introduces long range random connections in the bundle and the degree distributions $\rho(k)$ gets wide while average node degree $\langle k \rangle$ is kept constant $\langle k \rangle = 4$. Fig. 6.1($right$) presents the degree distribution of the network $\rho(k)$ for different rewiring probability values p at the system site $l = 1000$. For large p values, small clusters having few fibers and isolated fibers may appear due to rewiring. Such small clusters were excluded by picking up solely the largest cluster of nodes for further calculations.

The random strength σ_{th} where fibers fail, was sampled from a Weibull distribution given in Eq. (3.5). The Weibull distribution made it possible to control the amount of the strength disorder of fibers by varying the exponent m in Eq. (3.5) (see Fig. 3.2(a) for illustration). An important feature of the model is that fiber's strength σ_{th}^{i} and degree k_i $(i = 1, \ldots, N)$ are not correlated.

Under gradually increasing load, all fibers of the bundle initially keep the same load, so the fiber with lowest breaking threshold will break first. Assuming the nearest neighbor interaction, the load of a broken fiber is shared equally among its nearest unbroken neighbors on the underlying network. Local breaking threshold of neighboring fibers can be exceeded due to this updated load, resulting more failures which then again followed by load redistribution. Subsequent failure and step by step load redistribution results in failure cascade that is initiated by a single broken fiber and continues until all the load receiving fibers in a load redistribution step, can bear the increased load. This localized load sharing (LLS) implies that the fibers failed in an avalanche produce a joint cluster on underlying network, which has a high load concentration along its perimeter. There are two sources of disorder in the system, one is the random strength of fibers and other is random connections of underlying network, both are quenched. Both of them collectively produce an inhomogeneous stress field which grows as failure of system

proceeds. When fiber i with load σ_i breaks, its all n_i nearest intact neighbors get the load increment $\Delta\sigma_i = \sigma_i/n_i$, hence, the load σ_j of a j neighboring fiber in updated as $\sigma_j \to \sigma_j + \Delta\sigma_i$. Here $n_i \leq k_i$ holds, where node i has the initial degree k_i. External load remains constant during an avalanche hence load redistribution is the only source of failure spreading. External load is increased further after the avalanche stops to provoke the failure of the next fiber. Each intact fiber σ_i gets the same load increment $\delta\sigma$ so that $\sigma_i \to \sigma_i + \delta\sigma$ holds, where $\delta\sigma$ is estimated as the minimum difference between load σ_i and strength σ_{th}^i of surviving fibers $\delta\sigma = \min_i(\sigma_{th}^i - \sigma_i)$. System fails eventually when a load increment provoke a catastrophic avalanche that breaks all the surviving fibers.
For this study computer simulations were carried out starting from a square lattice with size $l = 400$ and $N = 160.000$ fibers, and periodic boundary conditions were used in both directions. To set the degree of strength disorder with the Weibull distribution, λ was fixed to 1, while varying m in the interval $1 \leq m \leq 22$. I examined 30 different p values from $0 \leq p \leq 1$. For each parameter set I calculated averages over 2000 samples.

6.2 Macroscopic response of fiber bundles on complex networks

To characterize the macroscopic behaviour of bundles, we need to determine the relationship of its stress σ and strain ε, i.e. the $\sigma(\varepsilon)$ constitutive relation. In the ELS limit, where all fibers are interacting with each other and bear the same load, Eq. (3.8) gives the analytical solution for this constitutive relation that is represented by the dotted line for $m = 1$ in Fig. 6.2(a). The constitutive curves in load controlled testing, can be realized only up to the maximum, where sudden failure takes place in the form of a catastrophic avalanche. , the critical stress σ_c and strain ε_c of the bundle can be defined by the value and position of

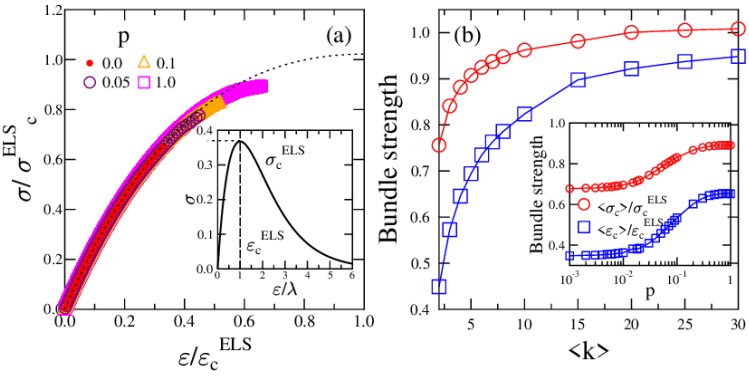

Figure 6.2: (a) Constitutive curves $\sigma(\varepsilon)$ of fiber bundle for various values of p compared to the analytical solution of Eq. (3.8) represented by dotted line for $m = 1$. Both axis are re-scaled by mean field critical strain ε_c^{ELS} and load σ_c^{ELS}. The inset presents the whole $\sigma(\varepsilon)$ curve of Eq. (3.8). (b) Main panel: Average critical strengths $\langle\varepsilon_c\rangle$ and $\langle\sigma_c\rangle$ at $p = 1$ as a function of $\langle k\rangle$ from $2 \leq \langle k\rangle \leq 30$. Inset: $\langle\varepsilon_c\rangle$ and load $\langle\sigma_c\rangle$ of network rescaled with their mean field counterparts, as a function of p at $m = 1$. Both figures have the same legend as provided in inset.

maximum of $\sigma(\varepsilon)$, respectively. In numerical simulations of finite bundles of LLS, we can obtain system's stress σ and strain ε at any topology by dividing sum of load σ_i of fibers (nodes) $F = \sum_{i=1}^{N} \sigma_i$ by bundle size $\sigma = F/N$ and by the total number of remaining fibers $\varepsilon = F/N_{intact}$, respectively.

Computer simulations for LLS on regular lattices proved that the constitutive curve of bundle obeys the mean field solution of Eq. (3.7) [20, 107]. However, more brittle response is observed as $\sigma(\varepsilon)$ curve ends earlier at low σ_c and ε_c close to initial elastic regime. Figure 6.2(a) illustrates that this response is valid for all the considered networks, but the constitutive curves approach the higher values of σ_c and ε_c, as p increases. For a better understanding of the effect of network structures on bundle strength, I calculated the average critical strengths $\langle\sigma_c\rangle$ and $\langle\varepsilon_c\rangle$ as a function of p. It is clear from inset of Fig. 6.2(b) for $m = 1$ that

for small p values, rewired contacts have hardly any effect on bundle strength, hence, both $\langle\sigma_c\rangle$ and $\langle\varepsilon_c\rangle$ keep their original values which are characteristic for the non rewired square lattice. When p surpasses a threshold value $p \gtrsim 0.01$ the strength starts increasing and saturates to a maximum value for fully randomized system $p \to 1$. Note that the strengths in figure are rescaled with their mean field (ELS) counterparts

$$\varepsilon_c^{ELS} = \frac{\lambda}{E}\left(\frac{1}{m}\right)^{1/m}, \tag{6.2}$$

$$\sigma_c^{ELS} = \lambda\left(\frac{1}{m}\right)^{1/m} e^{-1/m}, \tag{6.3}$$

obtained from Eq. (3.8). This comparison reveals that as random links start to dominate load transfer between fibers, bundle strength approaches to ELS limit but gets saturated at lower values. Because the average degree of interacting fibers is fixed to $\langle k\rangle = 4$ that can still produce a remarkable stress concentration on network, as a result, bundle's fracture strength reduces as compared to the ELS limit. I performed numerical simulations to confirm this argument on random graphs for $p = 1$ with the system size N as that of the original square lattice and varying the average node degree $\langle k\rangle$ in a wide range. Figure 6.2(b) shows convergence of $\langle\sigma_c\rangle$ and $\langle\varepsilon_c\rangle$ to their ELS counterparts by increasing $\langle k\rangle$ in a fully random network $p = 1$, as expected.

6.3 Avalanche size distribution

On micro-scale, failure of the bundle proceeds in cascades or avalanches of local failures which are triggered by a single breaking event. The avalanche size Δ is defined as the number of fibers failed in the avalanche. Statistics of avalanche activity can be characterized by size distribution of avalanches $p(\Delta)$, which revealed a strong dependence on the topology of network of load transmitting links. It is clear from Fig.

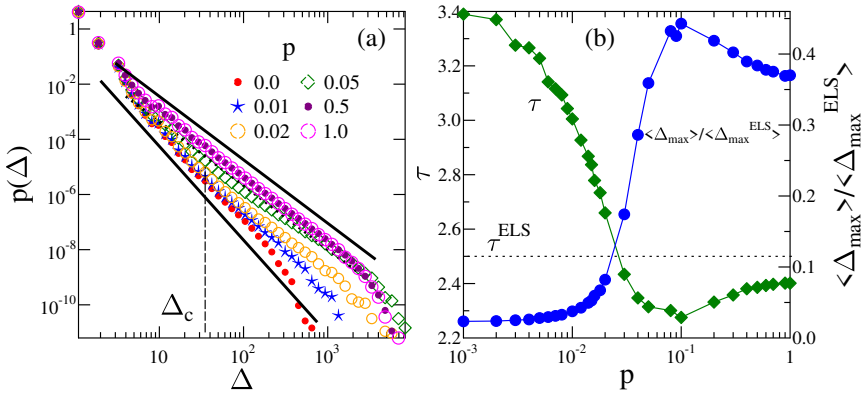

Figure 6.3: (*a*) Avalanche size distribution $p(\Delta)$ for different p values at $m = 1$. Power laws with exponents 3.4 and 2.3 are represented by two straight lines, for $p = 0$ and $p = 1$, respectively. (*b*) Left vertical axis: Power law exponent τ of $p(\Delta)$ as a function of p. Right vertical axis: Average of maximum avalanche $\langle \Delta_{max} \rangle$ re-scaled with its ELS counterpart $\langle \Delta_{max}^{ELS} \rangle$ as a function of p. Horizontal dashed line presents the MF value of avalanche size exponent $\tau^{ELS} = 5/2$.

6.3(*a*) that at $p = 0$, i.e. on a regular square lattice, where a strong spatial load localization dominates, the distribution $p(\Delta)$ can be approximated as a power law

$$p(\Delta) \sim \Delta^{-\tau}, \tag{6.4}$$

followed by a cutoff. The rather high value of exponent $\tau = 3.4 \pm 0.1$ is in good agreement with previous FBM studies [20, 107, 108].
Rapid fall of the distribution and low value of the cutoff burst size Δ_{max} prove that avalanches are usually small as compared to the system size N. On a regular lattice because of strong localization large size avalanches lead to sudden collapse of the bundle. The main effect of rewiring is that increasing p the number of long range connections increases, and hence, the stress concentration gradually decreases. Consequently, the system can sustain larger avalanches without suffering catastrophic failure. As a result, Δ_{max} increases and $p(\Delta)$ shows a

crossover to second regime of power law with relatively lower exponent. Smaller value of τ indicates a growth of the fraction of large size avalanches in failure dynamics of system as indicated in Fig. 6.3(a). The crossover burst size Δ_c, highlighted by the dashed vertical line in the figure, separates the two regimes of power law. The value of Δ_c depends on the rewiring probability p, i.e. by increasing p, Δ_c slowly shifts to smaller values and in the $p \to 1$ limit, almost a single power law remains with a notably lower exponent as compared to the original square lattice at $p = 0$. I characterized the evolution of $p(\Delta)$ by determining the average largest avalanche size $\langle \Delta_{max} \rangle$ and the exponent of the power law τ in large avalanche regime as a function p. Fig. 6.3(b) shows that up to a rewiring probability $p_l \approx 0.01$, cutoff avalanche size $\langle \Delta_{max} \rangle$ is almost constant, though the exponent τ bear some variations. This behaviour suggests that the small number of randomized connections has a insignificant effect on the avalanche failure dynamics in the $p \lesssim 0.01$ parameter range. However, when p_l is exceeded a fast change in avalanche size distribution occurs indicated by decreasing τ a increasing $\langle \Delta_{max} \rangle$. For high rewiring probability $p \to 1$, convergence of τ to a constant $\tau \approx 2.3$ was observed, that is very close to the MF exponent of burst size of FBMs $\tau^{ELS} = 5/2$ [18, 21]. The result implies that on remarkably randomized networks, avalanche failure statistics of localized load sharing FBM is almost equivalent to the universal MF class of the system, in agreement with macroscopic behaviour of the bundle's strength. The result is in good agreement with Ref. [19] where FBMs were investigated on Watts-Strogatz networks and in high rewiring probability range i.e. $p \geq 0.2$ recovering the MF behaviour.

One interesting thing to note in Fig. 6.3(b) is that the maximum of $\langle \Delta_{max} \rangle$ lies around $p^* \approx 0.1$ that coincides practically with the minimum of the exponent τ. This behaviour shows that a network topology exists determined by p^* at which networks can endure the largest avalanches with a significant frequency. The reason is that increasing p two effects

compete with each other: First, the growing randomness of network reduces the stress concentration. This process stabilizes the system so that avalanches can approach larger sizes without generating a catastrophic breakdown. However, at high p values an opposite effect occurs, i.e. a growing number of low degree fibers appears on the network, around them load localization increases, hence, making the system more vulnerable to avalanches. p^* provides the optimal value for avalanche tolerance of system.

6.4 Role of strength disorder in the localized to mean field transition

I performed a large number of simulations of failure dynamics of fibers' network at several values of Weibull exponents m varying the amount of strength disorder in a wide range. These simulations revealed a decisive role of the degree of strength disorder in the LLS-ELS transition. Figure 6.4(a) shows for the average critical load $\langle\sigma_c\rangle$ that when threshold disorder is decreased by increasing m, the beginning of the transition, i.e. the rewiring probability p_l at which the first clear deviation from LLS behaviour of regular lattice occurs, shifts to higher values. As an example, for $m = 7$, deviation starts at $p_l \approx 0.1$, that is much higher than the corresponding $p_l \approx 0.01$ value obtained at $m = 1$. This transition ends at the probability p_u above which bundle strength typically does not change. The p_u value also increases with decreasing strength disorder and goes to 1 such that the transition region shrinks. It can be seen that by increasing m, the asymptotic strength $\langle\sigma_c\rangle\,(p = 1)$ tends to decrease as compared to its corresponding ELS value σ_c^{ELS}, showing that randomization of the network structure at lower strength disorder provides less improvement of load bearing capacity of the system. An interesting point here is that at low disorders, starting from $m = 10$, we get non-monotonous $\langle\sigma_c\rangle\,(p)$ curves i.e. the onset of increase of system's

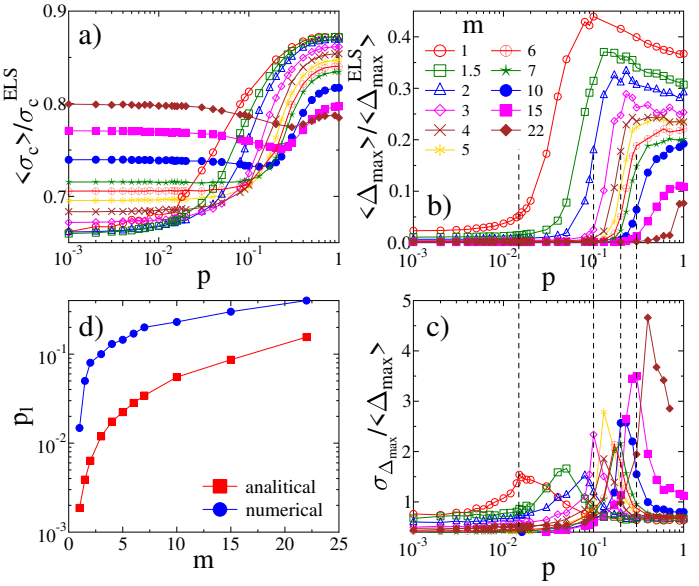

Figure 6.4: (a) Average critical load $\langle\sigma_c\rangle$ and (b) average of largest avalanche size $\langle\Delta_{max}\rangle$, re-scaled with their MF counterparts, as function of p for different m values. (c) The relative scatter of largest avalanche size, i.e. the standard deviation $\sigma_{\Delta_{max}}$ divided by average $\langle\Delta_{max}\rangle$ of the largest avalanche size. Legend for (a, b, c) is given in (b). (d) The rewiring probability p_l where LLS to ELS transition starts plotted as a function of m.

ultimate strength for $m = 10, 15$ is preceded by a local minimum. In addition, for $m = 22$, the limiting value of strength obtained at $p \to 1$ drops below the strength at $p = 1$. The result implies that when the strength of the elements of the system is sampled from a very narrow interval, rewiring causes reduction of bundle's strength at any value of the rewiring probability p.

The study of avalanche size statistics proved a similar effect of the threshold disorder of fibers on the LLS-ELS transition of the failure mechanism: it can be observed in Fig. 6.4(b) that as the degree of

strength disorder decreases with increasing m the average largest avalanche size $\langle \Delta_{max} \rangle$ keeps constant at its $p = 0$ value for a wide range of p. The estimated value of p_l i.e. the lower limit of transition regime is in agreement in Figs. 6.4(a) and 6.4(b) for macro and microscopic quantities confirming that p_l increases with increasing m. It is important here that the $\langle \Delta_{max} \rangle (p)$ curves grow sharper as compared to the bundle strength $\langle \sigma_c \rangle (p)$ showing the transition in a more transparent way. Large fluctuations of Δ_{max} can be expected at starting point of LLS-ELS transition. To give a quantitative characterization of this effect, Fig. 6.4(c) presents the relative scatter of Δ_{max}, i.e. ratio of its standard deviation $\sigma_{\Delta_{max}}$ and average $\langle \Delta_{max} \rangle$. For each value of m the curves have a well-defined maximum whose position sets the value of p_l. The vertical dashed lines in the figure for a few m values highlight that the peak of the relative scatter of Δ_{max} coincides well with the starting point of sharp rise of $\langle \Delta_{max} \rangle (p)$ in Fig. 6.4(b). It is of importance that as the threshold disorder decreases, the rewiring probability p^* of the position of the maximum of the $\langle \Delta_{max} \rangle$ curves, where networks sustain the largest cascades, shifts to higher values. Moreover, there is a gradual decrease in the value of the maximum and finally it disappears around $m \approx 4$ making the curves monotonically increasing. For strength disorder in the range $m > 4$, completely random graphs provide the highest tolerance of avalanches. In accordance with the response of the ultimate bundle strength, at lower threshold disorder of nodes, network randomization offers less improvement as compared to LLS limit. For each value of m, the avalanche size distributions $p(\Delta)$ undergo the same evolution as for $m = 1$ in Fig. 6.3(a): below p_l the avalanche size distribution remains practically the same as that of the original square lattice at $p = 0$. The power law regime with lower exponent appears for networks with $p \geq p_l$ along with the growth of the cutoff avalanche size $\langle \Delta_{max} \rangle$ and a slowly decreasing crossover avalanche size Δ_c. The transition is completed when p surpasses p_u, and a single power law of $p(\Delta)$ remains.

6.4.1 The onset of the LLS-ELS transition

To understand the emergence of the localized to mean field transition by varying p at different values of m, an analytical argument is constructed based on the change in the underlying network structure of load redistribution. On original regular lattice $p = 0$, an early failure of the whole bundle is easily driven by the strong localization of load on the perimeter of failed clusters [76, 107, 108]. Failed clusters in the last stable configuration are very small as compared to the size of system N, however, most of the fibers fail in last catastrophic avalanche. By adding long range random connections, the stress concentration decreases due to the growing perimeter of failed cluster. Hence the system can bear larger avalanches and its global load bearing capacity gets higher. At a given p value the average number of rewired links can be approximated as $2Np$ as each of the $2N$ initial links are rewired with probability p. Rewiring process effects a very small number of fibers at low p values, either by removal of nearest neighbor links or by a newly attached long range link. Hence, it can be assumed that at low p most of the avalanches have high chances to avoid fiber with rewired connections, however small avalanches have same statistics as that of original regular lattice at $p = 0$. Those avalanches, for which rewired connections are involved, can grow to large sizes and consequently follow a different statistics compared to the small ones. This mechanism is responsible for the crossover in the avalanche size distribution $p(\Delta)$ presented in Fig. 6.3(a).

To approximate the crossover burst size Δ_c, it is useful to determine the probability that an arbitrary node of the system is affected by rewiring. The probability that no one of the 4 nearest neighbor links of a fiber is rewired is $(1-p)^4$, whereas the probability of not being connected to any other fiber through a newly established link can be approximated as e^{-4p} for large N [109]. Consequently, the probability p_r that a randomly

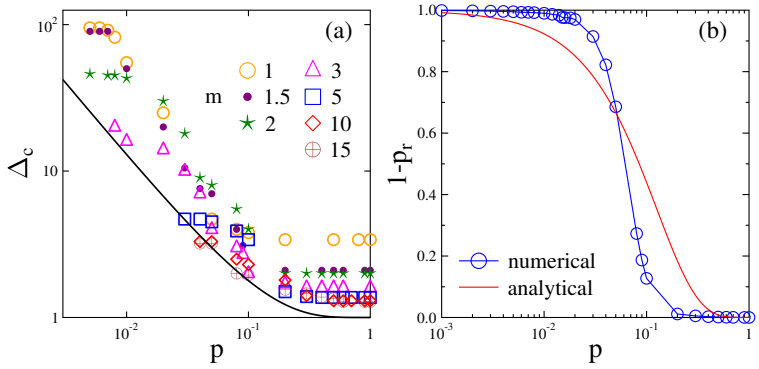

Figure 6.5: (*a*) Crossover burst size Δ_c. Symbols represent Δ_c obtained numerically at different Weibull exponents m, whereas the continuous curve is the analytical solution of Eq. (6.7). (*b*) Average fraction of fibers not affected by rewiring as a function of p compared to $1 - p_r$ from the solution of Eq. (6.5).

chosen node gets affected by rewiring can be written as

$$p_r = 1 - (1-p)^4 e^{-4p}. \tag{6.5}$$

Fig. 6.5(*b*) presents a comparison of the fraction of nodes not affected by rewiring obtained numerically in our system and the analytical result $1 - p_r$ obtained from Eq. 6.5. It can be seen that the analytical expression provides a reasonable description of the numerical data. I assumed that the crossover appears at an avalanche size Δ_c beyond which avalanches on the average contain at least one affected fiber by the rewiring process. This argument yields the expression

$$\Delta_c p_r(p) \approx 1, \tag{6.6}$$

from which the relation follows

$$\Delta_c \approx \frac{1}{p_r(p)}. \tag{6.7}$$

Note that for $p \to 0$ the value of Δ_c diverges $\Delta_c \to \infty$, whereas it goes to 1 for $p \to 1$. From this arguments it follows that at lower rewiring

probabilities $p \ll 1$, crossover avalanche size is greater than the average maximum avalanche $\langle \Delta_{max} \rangle (p = 0)$ at $p = 0$. As a result, practically there is no effect of rewiring on the statistics and dynamics of stable avalanches in this range of p. Consequently, there is no crossover, so the avalanche size distributions practically remain the same as that of the square lattice (see Fig. 6.3(a)). Crossover appears for those values of p for which the condition

$$\langle \Delta_{max} \rangle (p = 0, m) > \Delta_c(p) \tag{6.8}$$

holds. Note that $\langle \Delta_{max} \rangle$ at $p = 0$ has strength disorder dependence too. First this appears at lower bound p_l of transition regime

$$\langle \Delta_{max} \rangle (p = 0, m) = \Delta_c(p_l) \tag{6.9}$$

from where p_l can be estimated as a function of m. In $p > p_l(m)$ regime, the crossover avalanche size that separates the two regimes of power laws with different exponents, can be determined by Eq. (6.7). The minimum possible value of Δ_c I could identify in my numerical measurements is $\Delta_c \approx 1 - 3$, from which p_u the upper limit of the crossover regime can be estimated. Further increasing p beyond p_u there is no qualitative change in failure process hence the avalanche size statistics remains the same. The above arguments imply that the strength disorder dependence of LLS-ELS transition arises from the disorder dependence of the avalanche activity of the unperturbed regular lattice. For each m and p considered I numerically estimated the crossover point Δ_c of avalanche size distributions by determining the value of Δ at which the power laws, fitted in the small and large avalanche regimes, intersect each other. It can be seen in Fig. 6.5(a) that the numerical values of $\Delta_c(p)$ are underestimated by analytical curve calculated by Eq. (6.7), however, the functional form gives a good description of numerical calculations. In Figure 6.5(a), at any given disorder parameter m, the lower p_l and upper p_u bounds of the transition regime can be pointed out as the values of p

where crossover appears first, and Δ_c becomes constant, respectively. For more accurately estimating the transition regime, I numerically solved Eq. (6.9) for p_l by substituting the value of $\langle \Delta_{max} \rangle \, (p = 0)$ for each m value from computer simulations. Figure 6.4(d) compares this semi-analytical curve of p_l to the numerical one estimated as the position of maxima of relative scatter of Δ_{max} given in Fig. 6.4 (c). The numerical results are again underestimated by the analytical ones but both have same functional form. The values of p_u estimated from numerical results lies between 0.2 and 1.

6.4.2 Failure driven by low degree fibers

My simulations proved that the competition of two processes determines the micro- and macro-scale responses of loaded networks. At higher p values, the increasing randomness of the network structure causes a reduction of load localization in system. Due to this mechanism, the avalanche tolerance and network's load bearing capacity can increase on the whole, specially at high strength disorder of nodes, as shown in Fig. 6.4(a, b). however, as the degree distribution $\rho(k)$ gets broader with growing p, nodes with low degree appear inducing an opposite effect of increasing load localization on their failure. This effect becomes important at low threshold disorder of nodes, where a low degree node when fails, can very easily trigger catastrophic failure.
To quantify this process I characterized the amount of threshold disorder of nodes by determining the average of minimum $\left\langle \sigma_{th}^{min} \right\rangle$ and maximum $\langle \sigma_{th}^{max} \rangle$ breaking thresholds in the bundle. From N independent randomly selected numbers sampled from the same probability distribution p, the average of the largest and smallest values can be written as

$$\left\langle \sigma_{th}^{min} \right\rangle = P^{-1}\left(\frac{1}{N+1}\right), \quad \text{and} \qquad \langle \sigma_{th}^{max} \rangle = P^{-1}\left(1 - \frac{1}{N+1}\right), \tag{6.10}$$

where P^{-1} represents the inverse of cumulative distribution [1]. By

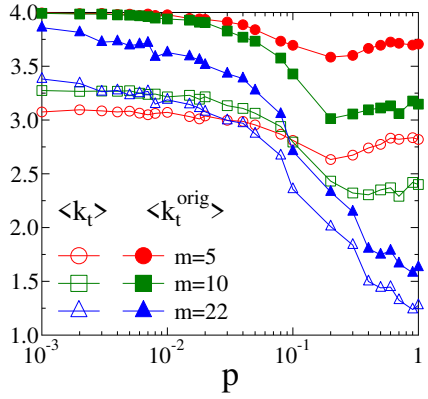

Figure 6.6: Average number of intact neighbors $\langle k_t \rangle$ (empty symbols) and average original degree $\left\langle k_t^{orig} \right\rangle$ (filled symbols) of the fiber whose failure triggers the final breakdown of the fiber network. Results for three values of m are included.

substituting the Weibull distribution from Eq. (3.5), the above equations take the simple form

$$\left\langle \sigma_{th}^{min} \right\rangle = \lambda \left(\frac{1}{N} \right)^{1/m}, \quad \text{and} \qquad \left\langle \sigma_{th}^{max} \right\rangle = \lambda \left(\ln N \right)^{1/m}. \tag{6.11}$$

The ratio of the two limit values r, gives a measure of the strength disorder of nodes

$$r = \left\langle \sigma_{th}^{max} \right\rangle / \left\langle \sigma_{th}^{min} \right\rangle = \left(N \ln N \right)^{1/m}. \tag{6.12}$$

The worst case for the stability of the fiber bundle is when a node with degree $k = 1$ has smallest breaking threshold σ_{th}^{min}, as it transfers its load to the neighbor when it fails. This load sharing will surely lead to the failure of neighbor if the increased load $2\sigma_{th}^{min}$ exceeds the largest breaking threshold σ_{th}^{max} in the bundle

$$2\sigma_{th}^{min} > \sigma_{th}^{max}. \tag{6.13}$$

As a huge load increment is introduced on the neighbors due to this secondary breaking event so we can assume that the avalanche can not stop and results in complete breakdown. Equation (6.13) implies that this process determines the behaviour of bundle only if the threshold distribution is noticeably narrow $r < 2$, and at sufficiently high rewiring probability p so to have a considerable number of nodes with degree $k = 1$. Using the relation of r from Eq. (6.12), Eq. (6.13) can be reformulated as a condition for Weibull shape parameter m

$$m > \frac{\ln(N \ln N)}{\ln 2}, \tag{6.14}$$

which gives $m > 20.9$ for our setup of the fiber bundle. It can be seen that highest value of m which I considered $m = 22$ satisfies the condition such that the eventual failure of network at this value of m must be mainly triggered by fibers with $k = 1$ at remarkably high rewiring probabilities. Fig. 6.6 supports this arguments, where $\langle k_t \rangle$ i.e. the average number of surviving neighbors of fibers whose failure trigger the catastrophic avalanche, is presented along with the average number of its original neighbors $\left\langle k_t^{orig} \right\rangle$. The figure shows that both quantities are decreasing with increasing p, i.e. when the degree distribution of nodes widens by increasing p, lower degree nodes trigger the failure. At high threshold disorder, i.e. low m, larger difference is observed between the original $\left\langle k_t^{orig} \right\rangle$ and final degrees $\langle k_t \rangle$ of triggering fibers, however, both curves switch to lower values and approach each other as disorder is reduced by increasing m. It is important to highlight that the $\left\langle k_t^{orig} \right\rangle$ and $\langle k_t \rangle$ curves both tend to 1, confirming that at low threshold disorder, nodes with the lowest degrees, make the system more vulnerable to failure cascades that trigger the catastrophic failure of the entire system. Most significant outcome of these findings is that the LLS-ELS transition is restricted to a range of strength disorder of nodes. At much low disorder the system becomes more vulnerable to avalanches preventing any improvement of avalanche tolerance and strength of the system. For

Weibull exponents satisfying the condition Eq. (6.14), there is no LLS-ELS transition.

6.5 Conclusion

I conducted a theoretical study of the failure dynamics of FBMs on complex networks with the goal to understand how the network topology of load transmitting connections along with the degree disorder of fiber's strength determines the micro- and macroscopic behaviour of system. My study was limited to one type of networks, i.e. the Watts-Strogatz rewiring technique was applied to interpolate between a completely regular square lattice and a completely random network. This choice had the advantage that detailed investigations could be carried out varying the degree of structural randomness of underlying network and the strength disorder of nodes. Based on computer simulations I demonstrated that a transition occurs from LLS to ELS behaviour of FBMs as the network of load transmitting connections is gradually randomized by rewiring. The transition is limited to a certain range of rewiring probability so that below the lower bound of the transition regime structural randomization has no significant effect on the failure dynamics, while above its upper bound the transition is completed, further rewiring does not change the behaviour of the system. In the transition regime avalanche size distribution displays a crossover behaviour between two power laws of different exponents. Increasing the rewiring probability, the critical stress and strain where eventual failure occurs, increase and tend to limits that are close to their mean field solutions. My computer simulations revealed that the threshold disorder of fibers has a notable effect on LLS to ELS transition: the transition regime becomes narrower and shifts to higher rewiring probabilities by decreasing the strength disorder of nodes. Most importantly, the transition is restricted to a well-defined range of strength disorder. More

specifically, there is a threshold amount of strength disorder of nodes below which rewiring does not improve the load bearing capacity nor the avalanche tolerance of system.

I pointed out that two competing mechanisms govern the network's response: rewiring of underlying network establishes long range random links in the load transmitting network that reduce the load localization and allows the system to bear larger avalanches. At low rewiring probabilities, due to the few long range connections, small sized avalanches remain unaffected. Above a characteristic size, avalanches involve more and more rewired fibers which increase their stability and result in a second power law regime of their size distribution with a lower exponent than for the small ones. However, with increasing structural randomness the degree distribution of the network widens increasing the fraction of low degree nodes. Hence, a counter effect emerges since the strong load localization around low degree nodes can trigger catastrophic failure making the system more vulnerable to early avalanches especially on highly randomized networks with a narrow distribution of node strength. I proposed an analytical description which captures the main ingredients of the above mechanism and provides a reasonable description of numerical results.

The failure mechanism of FBMs I analyzed is quite general in complex systems having four key elements: (I) the system's total load is incremented by adding same amount of load to all the intact elements; (II) nodes' failure is irreversible meaning that they are detached from the bundle along with their links without the possibility of healing; (III) failed nodes redistribute their load to their nearest surviving neighbors through the links; (IV) the load on the system is conserved during the propagation of failure cascades. FBMs have been used to investigate the emergence of avalanche failure of flow channels, roads carrying traffic and power grids. Due to a few additional assumptions we made, our results should be applicable for these modelling approaches, as well.

7 Chapter

Time evolution of failure avalanches

For cascading failure phenomena the avalanche size statistics is a primary source of information about the system. Recently, it has been demonstrated for Barkhausen noise in ferromagnetic materials and for crackling noise in fracture processes that the temporal profile of avalanches gives a deep understanding of dynamics of avalanche formation. Experiments revealed that Barkhausen pulses have a parabolic profile with left handed asymmetry, then theoretical studies clarified both the scaling relations and origin of asymmetry of avalanche profiles. In network science studies of models of information and diseases spreading, furthermore the neural networks showed that cascade profiles are highly sensitive to the network structure of the components of system. Most notably, the degree distribution of network was found to have a strong effect on temporal evolution of avalanches. Motivated by these recent results I investigated how the interplay of the topology of the load sharing network and of the stochastic strengths of connected elements governs the temporal evolution of avalanche failure in FBMs. Using the model of the previous section, I analyzed the average temporal profile of cascades and explored how the profiles shape changes as the

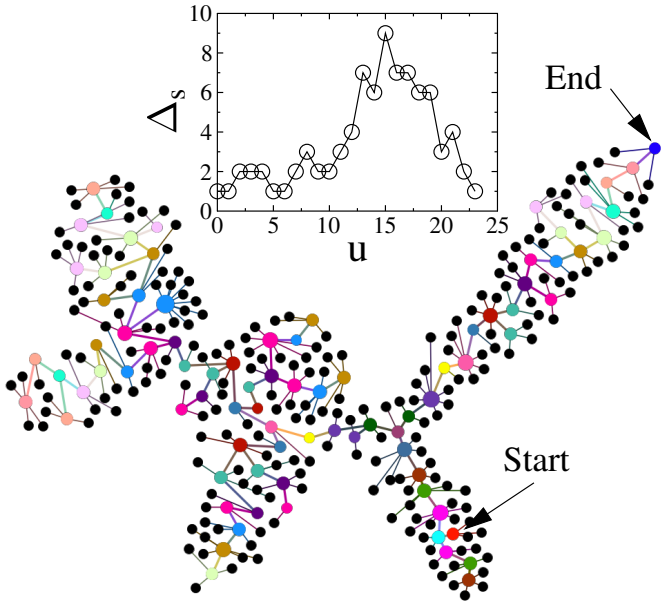

Figure 7.1: Spreading of an avalanche of size $\Delta = 84$ and duration 24, on a network of load transmitting connections at $p = 0.5$ with the Weibull exponent $m = 1$. The graph presents the temporal profile of avalanche.

structural randomness of the underlying network and the amount of strength disorder of nodes are varied. The details of the results discussed in this chapter are published in Ref. [29]

7.1 Statistics of avalanche duration

In the loading process of our FBM on any network topology the quasi-static loading guarantees that an avalanche always starts from the failure of a single fiber.
Due to load redistribution an additional Δ_s number of fibers may break, that defines a sub-avalanche of the evolving avalanche. To give a quantitative description of single avalanches I determined their size Δ and duration W as the total number of failed fibers and the number of

consecutive failure - load redistribution steps performed until the avalanche stops. Size of an avalanche Δ, the size of its sub-avalanches Δ_s, and the total duration W have the simple relation

$$\Delta = \sum_{u=1}^{W} \Delta_s(u), \tag{7.1}$$

where u is internal time variable of the avalanche or simply the integer index of sub-avalanches. The avalanche spreads over transmission network as it grows, which is illustrated in Fig. 7.1 for an event of size $\Delta = 84$ and duration $W = 24$. Arrows in the figure indicate that the avalanche starts and ends by a single fiber breaking. Black circles represent all load receiving nodes of the network and the large sized colored circles highlight those nodes that fail as a result of load sharing. Fibers belonging to the same sub-avalanche are indicated by the same color. Based on the consecutive colors, the evolution of the avalanche can easily be followed starting from the triggering fiber at the bottom of the figure. Note that the avalanche creates a connected cluster of failed fibers on network, but still fibers that break in the same sub-avalanche can show up far from each other. Note that the inset in the figure shows the temporal profile $\Delta_s(u)$ of the avalanche that will be discuss in detail later.
It has been discussed in Sec. 6.3 that the primary characteristics of the statistics of failure avalanches is the size distribution $p(\Delta)$, which have a strong dependence on network topology. To be able to make a direct comparison of $p(\Delta)$ and duration $p(W)$ of avalanches, Fig. 7.2(a) illustrates $p(\Delta)$ for Weibull exponent $m = 3$, where the same evolution of the distributions can be observed with increasing rewiring probability as before for $m = 1$.
Duration of a cascade is usually smaller than its size $W \leq \Delta$ so that equality is valid only when a single fiber fails in all sub-avalanches. It is clear from Fig. 7.2(b) that for the same parameters used in Fig. 7.2(a), the duration distribution of failure avalanches $p(W)$ has the same

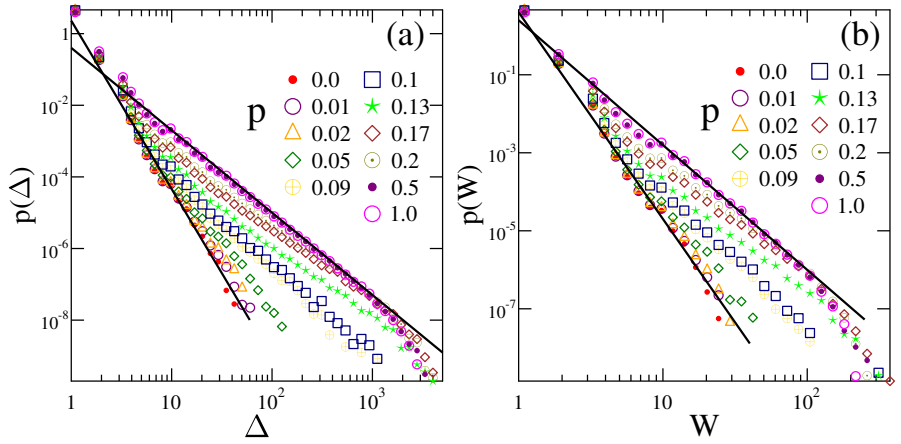

Figure 7.2: (a) Avalanche size distributions $p(\Delta)$ at various p values. The two straight lines are representing power laws with exponent values 2.3 and 4.7 for $p = 1$ and 0, respectively. (b) Duration distributions of failure avalanches $p(W)$. Power laws with exponents with 5.3 and 3.2 are represented by two straight lines. Both (a) and (b) are for the Weibull parameter $m = 3$. With increasing p an identical behaviour of crossover appears between two regimes of power law behaviour for both $p(\Delta)$ and $p(W)$.

qualitative behaviour as that of $p(\Delta)$ when p is varied: a power law distribution is evidenced for the regular square lattice at $p = 0$

$$p(W) \sim W^{-\tau_W}, \tag{7.2}$$

with a high exponent $\tau_W \approx 5.3$ indicating that long duration avalanches occur rarely in the failure dynamics. When long range random connections are established due to rewiring of the network, the system can bear larger cascades with longer duration, however, with growing p a crossover appears between two power law regimes of different exponents. With increasing p the crossover duration W_c shifts to smaller values. In the limit $p \to 1$ the crossover slowly disappears prevailing single power law of exponent $\tau_w \approx 3.2$ which is remarkably smaller than that of the

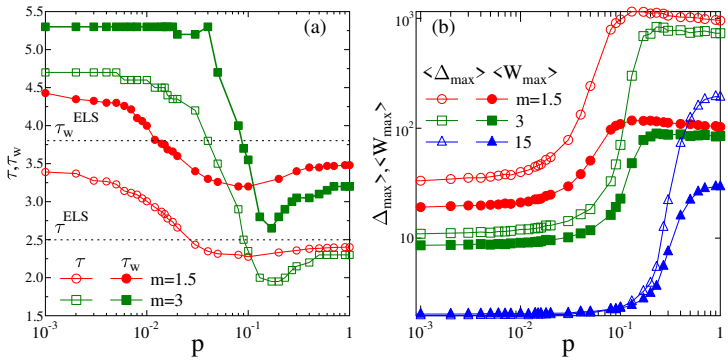

Figure 7.3: (a) Exponents τ and τ_W of $p(\Delta)$ and $p(W)$ of avalanches as a function of p for two values of m. Horizontal lines represent the MF values τ^{ELS} and τ_W^{ELS}. (b) Average maximum burst size $\langle \Delta_{max} \rangle$ and maximum duration $\langle W_{max} \rangle$ as function of p at three different m values.

regular lattice. It is notable that the duration distribution exponent τ_W is always higher than the exponent τ of size distribution. It is very informative to compare the evolution of the average maximum burst size $\langle \Delta_{max} \rangle$ and maximum duration $\langle W_{max} \rangle$ of avalanches, along with the power law exponents τ and τ_W obtained in the large avalanche regime, as the network is gradually randomized. Figures 7.3(a) and 7.3(b) present this comparison for two values of the Weibull exponent 1.5 and 3. It can be observed in the figures that up to a threshold rewiring probability $p_l(m)$ all the distinct quantities τ, τ_W, $\langle \Delta_{max} \rangle$, and $\langle W_{max} \rangle$ are almost constant and keep their $p = 0$ values. The result confirms again that in the $p \lesssim p_l$ parameter range the small number of randomized connections have a negligible effect on the evolution of failure avalanches. However, above p_l the failure process changes rapidly as shown by the sharp increase of both cutoff size $\langle \Delta_{max} \rangle$ and duration $\langle W_{max} \rangle$ of avalanches (Fig. 7.3(b)), and by fast decreasing exponents τ_w and τ (Fig. 7.3(a)). In the limit $p \to 1$ both exponents τ and τ_w approach to constants

$\tau_W \approx 3.2 - 3.5$ and $\tau \approx 2.3 - 2.4$ which are much close to their MF counterparts, i.e. $\tau^{ELS} = 5/2$ and $\tau_W^{ELS} \approx 3.8$. These results indicate that when the load transmission network is sufficiently randomized, the size and duration statistics of failure avalanches of LLS fiber bundle model becomes analogous to the system's MF universality class. The behaviour of the avalanche duration, that is the evolution of τ_W and the cutoff value W_{max} confirms the results of the previous chapter that gradually increasing the value of p a transition from LLS to ELS occurs in the system which starts at a threshold value p_l and gets completed at an upper bound p_u of rewiring probability after which there is no significant change in characteristic quantities of system [28].

In Figure 7.3(a) the comparison of exponents τ and τ_W at two different values of the Weibull parameter m demonstrates again that the strength disorder of fibers plays an important role in the evolution of avalanche statistics during the transition from LLS to ELS: outside the ELS regime, i.e. $p < p_u(m)$, the exponents τ_W and τ and are not universal, meaning that at low disorder both exponents become larger, meanwhile the difference between them decreases. On the other hand, with increasing p both τ and τ_W obtained at different m, show convergence towards the same universal ELS values τ^{ELS} and τ_W^{ELS}. As strength disorder decreases with increasing m both the lower p_l and upper bound p_u of the transition regimes shifts to higher rewiring probabilities which indicates that at low structural disorder of network a higher strength disorder of the nodes is required to realize the LLS to ELS transition. It has been presented in Fig. 6.3 that the avalanche size exponent τ has a minimum at a specific rewiring probability $p^*(m)$. In Fig. 7.3(a) the same behaviour is obtained for the duration exponent τ_W in such a way that the location of the minima of the curves of τ and τ_W coincide. The result confirms that the network topology obtained at p^* gives the highest stability at which the system can sustain largest avalanches with the longest duration without collapsing. At lower strength disorder, the local

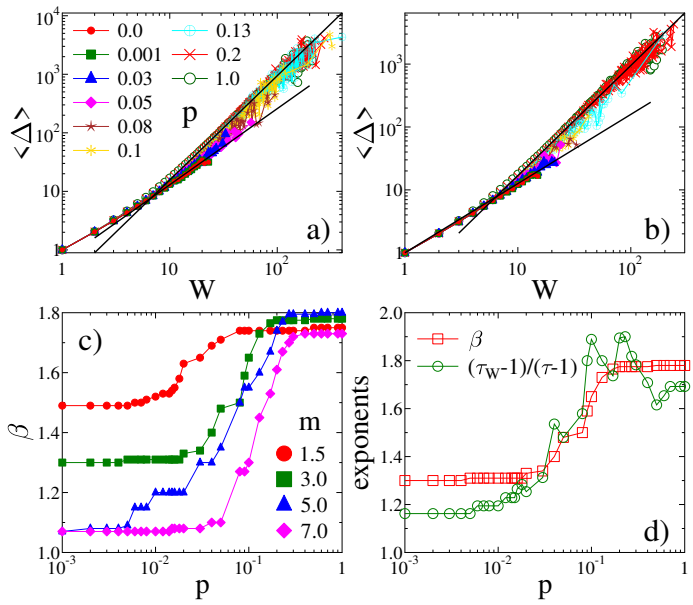

Figure 7.4: Average avalanche size $\langle\Delta\rangle$ as a function of duration W at different values of p for $m = 3$ (a) and $m = 5$ (b). (c) The exponent β as a function of p at different m values. (d) Test of the scaling relation Eq. (7.4) for $m = 3$.

minima of the exponents become sharp and deep as compared to their $p \to 1$ limit values showing that the LLS to ELS transition becomes more abrupt.

Figure 7.3(b) presents that the average maximum burst size $\langle\Delta_{max}\rangle$ and the maximum duration $\langle W_{max}\rangle$ show the same qualitative evolution as that of τ and τ_W with growing rewiring probability p. For each amount of strength disorder m both cutoffs are increasing as a function of p implying that at higher structural randomness avalanches with larger size and longer duration can be tolerated by the network. Nonetheless, the growth of the avalanche size is faster than duration, which shows that sub-avalanches become larger with increasing p. It is to be noted that at

lower values of p, when increasing m reduces strength disorder, the difference of $\langle \Delta_{max} \rangle$ and $\langle W_{max} \rangle$ slowly disappears. This indicates that sub-avalanches commonly consist of $1-2$ failing fibers in this parameter regime, however, the difference of these two curves again becomes higher when p is increased.
Of course, at a given parameter set long duration avalanches have a longer size but the relation between two quantities can depend on both the strength disorder of nodes and structure of underlying load transmitting network and on the . To evaluate this relation I calculated the average avalanche size $\langle \Delta \rangle$ at a fixed duration. Figure 7.4(a) shows that for $m = 3$ and at each p value the average avalanche size $\langle \Delta \rangle$ increases as a power law of duration

$$\langle \Delta \rangle \sim W^{\beta}, \tag{7.3}$$

whereas, exponent β depends on rewiring probability p. At lower p in the limit $p < p_l$, where the failure process is close to LLS class, the avalanche size increases gradually with duration, and hence we obtained $\beta = 1.3 \pm 0.08$ by fitting. For higher p values $p > p_l$, where avalanche spreading is dominated by long range links, a crossover can be noticed: small cascades, unaffected by the rewired connections, are still characterized by LLS value of β. However, above a characteristic value of duration W_c a sharp increase appears with a higher value of exponent which slowly increases with p. In the $p \to 1$ limit I obtained $\beta = 1.78 \pm 0.12$, which is very close to the MF value of $\beta^{ELS} \approx 2$. For a lower value of strength disorder i.e. $m = 5$, in Fig. 7.4(b) the same qualitative behaviour is obtained, however, similar to the avalanche size τ and duration τ_W exponents, β also proved to be universal only in the ELS limit obtained for sufficiently large rewiring probabilities $p > p_u$. On network of low structural randomness $p < p_u$, exponent β depends on the degree of strength disorder m. Particularly, in Fig. 7.4(b) I got $\beta = 1.77$ for $p = 1$, whereas in LLS limit $p = 0$, the value of $\beta = 1.1$ is remarkably

lower than for $m = 3$. For better understanding of the effect of degree of strength disorder on β, I determined its value by carefully fitting the $\langle\Delta\rangle(W)$ curves for each p value. It can be seen in Fig. 7.4(c) that the qualitative evolution of the β curves is consistent with the results of duration and size distributions of avalanches. In the ELS limit $p > p_u(m)$ the value of β is same for all m values with the error bars $\sigma_\beta \approx 0.1$. As by increasing m the strength disorder gets reduced, the LLS value of β shifts to lower values and approaches to 1 confirming that at low strength disorders, sub-avalanches mainly consists of single breaking fibers hence the avalanche size increases linearly with duration. Certainly, the three exponents τ, β, and τ_W of avalanche size and duration are not independent of each others, one can easily show that the scaling relation

$$\beta = \frac{\tau_W - 1}{\tau - 1}, \tag{7.4}$$

must hold among them [110]. Figure 7.4(d) represents the two sides of Eq. (7.4) plotted against p for $m = 3$. There is a suitable agreement between the two curves which proves the accuracy of our numerical findings. An important outcome of the computer simulations is that the scaling relation of Eq. (7.4) is fullfilled at any value of m and at all network typologies p. Note that in the range of much lower disorder $m \gg 1$ as β goes to 1 in LLS limit, the exponents of avalanche size and duration should approach the same limit value such that $\tau_W = \tau$ follows for $p < p_l(m)$.

7.2 Temporal profile of avalanche spreading

Cascades spread by a sequence of sub-avalanches that have a strongly fluctuating size Δ_s. The spatial spreading of a failure avalanche has been illustrated in Fig. 7.1 along with its temporal profile. Here Fig. 7.5 provides further examples of the stochastic nature of the temporal evolution $\Delta_s(u)$ $(u = 1, \ldots, W)$ of avalanches presenting the profile of

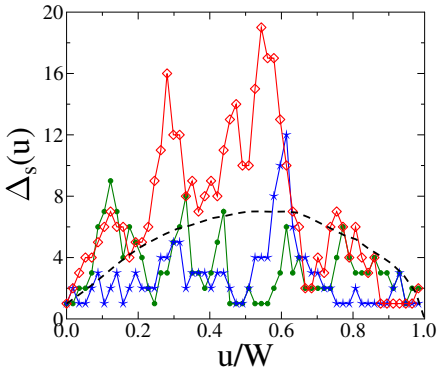

Figure 7.5: Evolution of single avalanches at $p = 0.5$. The sub-avalanche size $\Delta_s(u)$ is plotted for three events of the same duration $W = 57$ in this way that u is re-scaled with W. Dashed line represents the temporal profile averaged over 150 avalanches of same duration.

three events of a fixed duration $W = 57$ on a network at $p = 0.5$. In spite of the strong fluctuations of the $\Delta_s(u)$ curves of single avalanches, simulations proved that the average temporal profile $\langle \Delta_s(u) \rangle$ obtained by averaging over avalanches of a fixed duration W has a well-defined parabolic shape (see Fig. 7.5). Figure 7.6 compares avalanche profiles $\langle \Delta_s(u, W) \rangle$ at the same duration W with different p values. It can be seen that when p increases the sub-avalanche size increases, hence, the avalanche size Δ grows at same value of duration W. This result reveals that due to the existence of long range connections, avalanches of same duration can spread over a wider area of the bundle before catastrophic failure. Note that for all values of p and duration W the profiles have a parabolic form with a definite right handed asymmetry. As the sub-avalanche size is the rate of increase of the avalanche size, the asymmetry shows that the spreading of avalanches starts slowly then speeds up and finally stops suddenly. It can be deduced from Fig. 7.6 that at $p = 0$, i.e. on the regular square lattice, asymmetry is the highest,

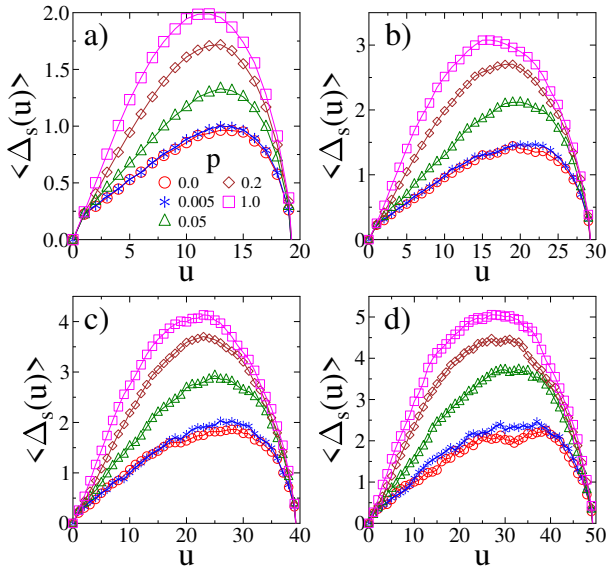

Figure 7.6: Temporal profile of failure avalanches $\langle \Delta_s(u, W) \rangle$ at a given duration W and $m = 1.5$. Profiles of fixed duration are compared at different values of p for W: (a) 20, (b) 30, (c) 40, (d) 50.

which then keeps decreasing with growing p. Note that the asymmetry holds up to some extent even in the range $p \to 1$, when the network of load transmitting connections becomes completely random.

My numerical analysis revealed that the degree of asymmetry is characteristic of network structure because at a given p its value is same for all the avalanches irrespective of their duration. This is illustrated in Fig. 7.7 for $m = 1.5$ where by rescaling the avalanche profiles $\langle \Delta_s(u, W) \rangle$ with a suitable power α of duration W, profiles of different durations W fall on the top of each other. This satisfactory data collapse proves the

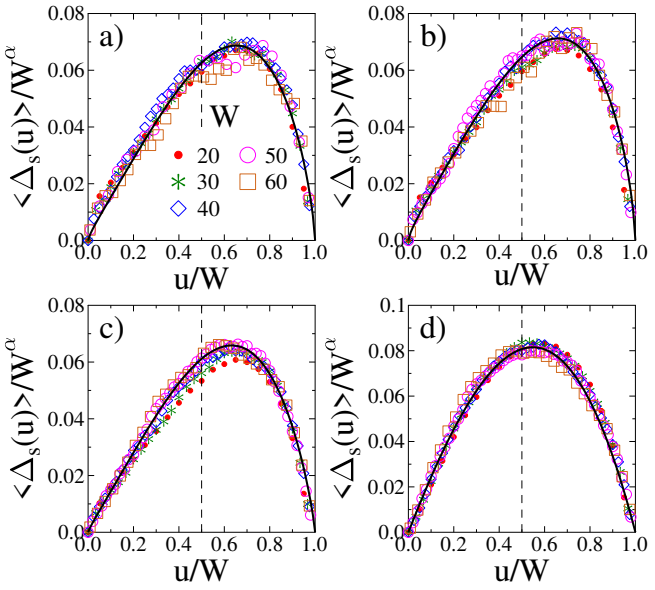

Figure 7.7: Scaling of temporal profile of avalanches at fixed p values : (a) 0, (b) 0.005, (c) 0.05, (d) 1 for $m = 1.5$. Vertical dashed lines represent the position of the mid-point of the interval $[0, 1]$. The continuous bold lines are fitting curves of the scaling function with Eq. (7.6).

validity of scaling structure of profiles

$$\langle \Delta_s(u, W) \rangle = W^{\alpha} f(u/W), \tag{7.5}$$

where the scaling function $f(x)$ and exponent α both depend on network structure p. Value of α in the figure falls between 0.65 and 1. Scaling analysis makes it clear that the avalanche profiles of random networks at $p = 1$ are not fully symmetric (see Fig. 7.7(d)), despite the symmetric parabolic form of avalanches in ELS fiber bundles [16, 82]. For a quantitative description of the evolution of degree of asymmetry with the

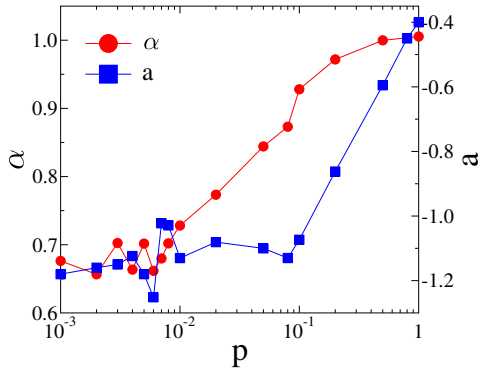

Figure 7.8: Shape parameters of cascade profiles a (right axis) and α (left axis), for $m = 1.5$.

rewiring probability p, I fitted the scaling function $f(x)$ with the relation

$$f(x) \sim [x(1-x)]^{\alpha} \left[1 - a(x - 1/2)\right], \tag{7.6}$$

which has been suggested in Ref. [110] based on experimental studies of the intermittent dynamics of inter-facial crack propagation. It is important to note that the parameter α is same as in Eq. (7.5). Parameter a controls the degree of asymmetry so that $a = 0$ implies symmetry, whereas positive and negative values mark left and right handed asymmetry, respectively. It is clear from Fig. 7.7 that Eq. (7.6) gives a good fitting quality of the scaling functions $f(x)$ for all p values. Figure 7.8 shows the dependence of the asymmetry parameter a and the exponent α on p for $m = 1.5$. α determines how flat is the profile around its maximum and how much the curve is round near the interval limits $u/W = 0$ and $u/W = 1$ without influencing the symmetry. More closer α is to 1, the profile shape becomes more parabolic [16, 82, 110]. Moreover, the position of the maximum is mainly controlled by parameter a without altering the overall shape of profile curves. Figure 7.8 illustrates that at $p = 0$, α starts in the vicinity of 0.65 and gradually increases to 1

at $p = 1$, which implying that the avalanche profile tends to the simple parabolic form of ELS bundles when the load transmitting network becomes completely random. however, the asymmetry parameter grows from $a \approx -1.0$ to $a \approx -0.4$ by increasing p, such that it remains negative even at $p = 1$ showing that some degree of asymmetry survives on fully random networks. The evolution of α with p is comparatively similar to the behaviour of other exponents τ_W, τ and β showing the LLS to ELS transition. However, the value of a remains constant keeping its LLS value roughly up to the upper bound of transition regime p_u, and then starts increasing continuously until $p = 1$ is reached. It follows from scaling law Eq. (7.5) that the average cascade size $\langle\Delta\rangle$ increases as a power law of duration $\langle\Delta\rangle \sim W^{1+\alpha}$, as already expressed in Eq. (7.3). Comparing the two expressions the relation of the exponents α and β can be deduced $\beta = 1 + \alpha$. This relation is valid to a good precision when comparing α and β obtained from Eq. (7.6) and by fitting of the average avalanche size as a function of W in Fig. 7.4, respectively. Scaling analysis of average temporal profile of failure avalanches requires a large number of avalanches at relatively higher durations. However, as the fiber's strength disorder decreases, both duration and avalanche size distribution become steeper which dramatically reduces the number of large avalanches of longer duration, hence, profiles analysis becomes difficult at low disorder. That's why I presented the results on avalanche profiles for a single value of m in the limit of high strength disorder.

7.3 Conclusions

I presented a comprehensive study of temporal evolution of the spreading process of failure avalanches in FBMs focusing on the degree of strength disorder of fibers and the role of underlying network structure of load transmitting connections. These calculations showed that not only the size Δ but also the duration W of failure avalanches has a scale free

statistics: on a regular square lattice $p = 0$ the duration W of avalanches is power law distributed with a rather high exponent τ_W and low cutoff value. The result shows that when load concentration is strong large avalanches of long duration occur very rarely in the system. Decreasing the strength disorder of fibers, both the duration and size exponents τ, τ_W increase and tend towards a common limit value. Increasing the structural randomness of the load transmission network with increasing p, exponents τ_W and τ decrease and approach their MF values, which do not depend on the degree of strength disorder of nodes of the network. Simulations showed that longer avalanches have larger size expressed by power law relation with an exponent β. For all values of p the exponents τ, τ_W, and β proved to follow a scaling relation with a good precision.

I showed that the average temporal profile of failure avalanches at all p values is a distorted parabola having a right handed asymmetry. The result implies that avalanches start gradually then speed up and finally stop suddenly. Simulations showed that as p increases more and more, avalanches of same duration evolve to large sizes and the degree of asymmetry of profiles decreases. At a given network topology p, I showed that profiles with different durations W can collapse on the top of each other by applying a scaling transformation. The result proves that asymmetry in profile curves is an attribute of network structure. It is interesting that even in the completely random regime of networks $p \to 1$ some degree of profile asymmetry prevailed.

Average temporal profile of avalanche failure has been studied numerically and analytically on complex networks in Ref. [111]. Using maximally random networks (generated e.g. by the configuration model [50]), it was demonstrated that asymmetric profiles usually emerge when degree distribution is fat-tailed. A left-handed asymmetry was observed, predicting a quick start and a slowly decreasing deceleration towards stopping. Results of my fiber bundle study can be compared to these results only in the range of $p \to 1$. I infer that the right handed

asymmetry that I observed can be attributed to the to the way of load redistribution and different degree distributions.

8 Chapter

Summary

In the framework of my PhD research I investigated failure phenomena emerging in complex systems which are composed of a large number of interacting elements. My research was focused in two main directions: First, I tried to obtain a deeper understanding of the phase transition analogy of fracture processes. For this purpose I studied how a solid body perforates due to dynamic impact loading as the energy of impact is varied at different amounts of materials' disorder. As the next step, I focused on the cascading failure mechanism driven by load redistribution on complex networks with the aim to understand how the interplay of the topology of the network of load transmitting connections and the disordered local strength affects the statistical and dynamical features of failure cascades. Based on analytical calculations and computer simulations I explored the complexity of these problems and obtained novel results which were published in 3 papers.

To investigate the impact induced failure of a bar shaped specimen of heterogeneous materials I constructed a simple model of three-point bending. Varying the energy of impact and the amount of disorder of the material I analyzed in details how breaking of the bar occurs due to a hit in the middle. I showed that depending on the imparted energy the impact process has two different outcomes: there exists a critical impact

energy below which the specimen gets damaged in the sense that it suffers partial failure and keeps its integrity, while above the critical point perforation occurs and the specimen breaks into two pieces. Computer simulations revealed that this damage to perforation transition has analogies to continuous phase transitions characterized by critical power laws.

I performed a careful numerical analyzes to determine the critical exponents of the phase transition. In particular, I identified the fraction of intact interface and the deflection rate as the order parameter and susceptibility of the damage to perforation transition, respectively, and determined their critical exponents. I showed that at finite disorder different exponents are obtained farther and closer to the critical point and explained this crossover in terms of the geometrical structural of damage.

I deduced scaling laws of the damage threshold and critical deflection of the system in terms of the amount of disorder and number of fibers used for discretization in the model of three-point bending. I demonstrated that if the number of fibers is sufficiently high the results are independent of the details of discretization.

As to the next, I carried out a theoretical study of the failure dynamics of the fiber bundle model on complex networks with the goal to understand how the interplay of the topology of the network of load transmitting connections and of the amount of disorder of the strength of fibers determines the behaviour of the system both on the micro- and macro-scales. My study was limited to one type of networks, i.e. the Watts-Strogatz rewiring technique was applied to interpolate between a completely regular square lattice and a completely random network. I demonstrated that a transition occurs from the localized to the mean field behaviour of FBMs as the network of load transmitting connections is gradually randomized by rewiring. The transition is limited to a range of the rewiring probability so that below the lower bound of the transition

regime structural randomization has no significant effect on the failure dynamics, while above its upper bound the transition is completed. In the transition regime the avalanche size distribution displays a crossover between two power laws of different exponents. Increasing the rewiring probability, the critical stress and strain where eventual failure occurs, increase and tend to limits that are close to their mean field values.

I pointed out that two competing mechanisms govern the network's response: rewiring of the underlying network establishes long range random links in the load transmitting network that reduce the load localization and allows the system to bear larger avalanches. However, with increasing structural randomness the degree distribution of the network widens increasing the fraction of low degree nodes. Hence, a counter effect emerges since the strong load localization around low degree nodes can trigger catastrophic failure making the system more vulnerable to early avalanches especially on highly randomized networks with a narrow distribution of node strength. I proposed an analytical description which captures the main ingredients of the above mechanism and provides a reasonable description of the numerical findings.

My computer simulations revealed that the threshold disorder of fibers has a substantial effect on the LLS to ELS transition: the transition regime becomes narrower and shifts to higher rewiring probabilities by decreasing the strength disorder of nodes. Most importantly, the transition is restricted to a well-defined range of strength disorder: there exists a threshold amount of strength disorder of nodes below which network randomization does not provide any improvement neither of the load bearing capacity nor of the avalanche tolerance of the system. I identified an optimal network structure with the highest robustness against cascading failure.

To continue the investigations, I performed a comprehensive study of the temporal evolution of the spreading process of failure avalanches driven by the gradual redistribution of load in the fiber bundle model focusing

on the role of the underlying structure of the load transmitting network and the degree of strength disorder of fibers. My calculations revealed that not only the size but also the duration of failure avalanches has a scale free statistics: at low structural disorder when load concentration is strong, large avalanches of long duration occur very rarely in the system. Decreasing the strength disorder of fibers, both the duration and size exponents increase and tend towards a common limit value. Increasing the structural randomness of the load transmission network, the exponents decrease and approach their mean field values, which do not depend on the amount of strength disorder of nodes of the network. Simulations showed that longer avalanches have a larger size expressed by a power law relation. I demonstrated that at any rewiring probability the exponents of avalanche size, duration, and their correlation obey a scaling relation.

I showed that the average temporal profile of avalanches on all network topologies is a distorted parabola having a right handed asymmetry. The result implies that avalanches start slowly then speed up and finally stop suddenly. My simulations showed that as the network becomes more and more random, avalanches of the same duration evolve to larger sizes and the degree of their profile's asymmetry decreases. I demonstrated that at a given network topology, profiles of different duration can be collapsed on the top of each other by means of a scaling transformation. The result proves that the degree of asymmetry of avalanche profiles is an attribute of the network structure.

9 Chapter

List of publications

Papers in refereed journals

P1 A. Batool, G. Pal and F. Kun, *Impact-induced transition from damage to perforation*, Phys. Rev. E **102**, 9 (2020). **IF: 2.529**

P2 A. Batool, G. Pal, Z. Danku, and F. Kun, *Transition from localized to mean field behaviour of cascading failures in the fiber bundle model on complex networks*, Chaos Solit. Fractals **159**, 112190 (2022). **IF: 9.992**

P3 A. Batool, G. Pal, Z. Danku, and F. Kun. *Temporal evolution of failure avalanches of the fiber bundle model on complex networks.* Chaos **32**, 063121 (2022). **IF: 3.741**

Talks

T1 A. Batool, *Transition from localized to mean field behaviour of cascading failures in the fiber bundle model on complex networks*, Avalanche 2022, Debrecen, Hungary, 29.8-2.9.2022.

Posters

PT1 A. Batool, G. Pal and F. Kun, *Failure avalanches on complex networks*, 46th Conference of the Middle European Cooperation in Statistical Physics (MECO46), Riga, Latvia, 11-13.05.2021.

Bibliography

[1] A. Hansen and S. Roux, *Statistical toolbox for damage and fracture, in: D. Krajcinovic and J. V. Mier (Eds.), Damage and Fracture of Disordered Materials*, (Springer Verlag, 2000) No. 410 in CISM Courses and Lectures, chapter 2, 17–101.

[2] S. Biswas, P. Ray, and B. K. Chakrabarti, *Statistical Physics of Fracture, Breakdown, and Earthquake: Effects of Disorder and Heterogeneity*, Statistical Physics of Fracture and Breakdown (John Wiley & Sons, New York, 2015).

[3] H. J. Herrmann and S. Roux, eds. *Statistical models for the fracture of disordered media, Random materials and processes*, (Elsevier, Amsterdam, 1990).

[4] I. Dobson, B. A. Carreras, V. E. Lynch and D. E. Newman, *Complex systems analysis of series of blackouts: Cascading failure, critical points, and self-organization*, Chaos **17**, 026103 (2007).

[5] C. A. Andresen, A. Hansen, R. L. Goc, P. Davy and S. M. Hope, *Topology of fracture networks*. Front. Phys. **1**, 7 (2013).

[6] O. Yagan, *Robustness of power systems under a democratic-fiberbundle-like model*, Phys. Rev. E **91**, 062811 (2015).

[7] J. M. R. Barredo, D. E. Newman, B. A. Carreras and I. Dobson,

The interplay of network structure and dispatch solutions in power grid cascading failures, Chaos **26**, 113111 (2016).

[8] M. Frasca, L. V. Gambuzza, *Control of cascading failures in dynamical models of power grids*, Chaos, Solitons & Fractals **153**, 111460 (2021).

[9] S. Biswas, L. Goehring, *Load dependence of power outage statistics*, Europhys. Lett. **126**, (2019) 44002.

[10] D. Sornette, *Predictability of catastrophic events: Material rupture, earthquakes, turbulence, financial crashes, and human birth*, Proc. Natl. Acad. Sci. USA **99**, 2522 (2002).

[11] M. J. Alava, et al., *Role of Disorder in the Size Scaling of Material Strength*, Phys. Rev. Lett. **100**, 055502 (2008).

[12] J. V. Andersen, D. Sornette, and K. -T. Leung, *Cricritical Behavior in Rupture Induced by Disorder*, Phys. Rev. Lett. **78**, 2140 (1997).

[13] C. B. Picallo, et al., *From Brittle to Ductile Fracture in Disordered Materials*, Phys. Rev. Lett. **105**, 155502 (2010).

[14] E. Karpas and F. Kun, *Disorder-induced brittle–to–quasi-brittle transition in fiber bundles*, Europhys. Lett. **95**, 16004 (2011).

[15] Y. Moreno, J. B. Gomez and A. F. Pacheco, *Fracture and Second Order phase transitions*, Phys. Rev. Lett. **85**, 2865 (2000).

[16] Z. Danku and F. Kun, *Temporal and spacial evolution of bursts in creep rupture*, Phys. Rev. Lett. **111**, 084302 (2013).

[17] A. Hansen, P. Hemmer, and S. Pradhan, *The Fiber Bundle Model: Modeling Failure in Materials*, Statistical Physics of Fracture and Breakdown, (Wiley, New York, 2015).

[18] R. C. Hidalgo, F. Kun, K. Kovács, and I. Pagonabarraga, *Avalanche dynamics of fiber bundle models*, Phys. Rev. E **80**, 051108 (2009).

[19] D. -H. Kim, B. J. Kim and H. Jeong, *Universality class of the fiber bundle model on complex networks*, Phys. Rev. Lett. **94**, 025501 (2005).

[20] R. C. Hidalgo, Y. Moreno, F. Kun and H. J. Herrmann, *Fracture model with variable range of interaction*, Phys. Rev. E **65**, 046148 (2002).

[21] M. Kloster, A. Hansen, P. C. Hemmer, *Burst avalanches in solvable models of fibrous materials*, Phys. Rev. E **56**, 26152625 (1997).

[22] F. Kun, F. Raischel, R. C. Hidalgo and H. J. Herrmann, *Extensions of fiber bundle models, in: P. Bhattacharyya, B. K. Chakrabarti (Eds.), Modelling Critical and Catastrophic Phenomena in Geoscience. A Statistical Physics Approach*, Lecture Notes in Physics, (Springer-Verlag Berlin Heidelberg New York, 2006) 57–92.

[23] A. Batool, G. Pal and F. Kun, *Impact-induced transition from damage to perforation*, Phys. Rev. E **102**, 9 (2020).

[24] B. K. Chakrabarti, *A fiber bundle model of traffic jams*, Physica A **372**, 162 (2006).

[25] J. -F. Zheng, Z. -Y. Gao, X. -M. Zhao, B. -B. Fu, *Extended fiber bundle model for traffic jams on scale-free networks*, Int. J. Mod. Phys. C **19**, 1727 (2008).

[26] C. Barre, J. Talbot, *Cascading blockages in channel bundles*, Phys. Rev. E **92**, (2015) 052141.

[27] B. K. Chakrabarti, S. Biswas, and S. Pradhan, *Cooperative dynamics in the fiber bundle model*, Front. Phys. **8**, 664 (2021).

[28] A. Batool, G. Pal, Z. Danku, and F. Kun, *Transition from localized to mean field behaviour of cascading failures in the fiber bundle model on complex networks*, Chaos Solit. Fractals **159**, 112190 (2022).

[29] A. Batool, G. Pal, Z. Danku, and F. Kun, *Temporal evolution of failure avalanches of the fiber bundle model on complex networks*, Chaos **32**, 063121 (2022).

[30] A. A. Griffith, *The phenomena of rupture and flow in solids*, Philos. T. Roy. Soc. A **221**, 163 (1921).

[31] G. R. Irwin, *Analysis of Stresses and Strains Near the End of a Crack Traversing a Plate* , J. Appl. Mech. **24**, 361 (1957).

[32] Z. P. Bazant, *Scaling theory for quasibrittle structural failure*, Proc. Natl. Acad. Sci. U.S.A. **101**, 13400 (2004).

[33] M. J. Alava, P. K. V. V. Nukala and S. Zapperi, *Statistical models of fracture*, Adv. Phys. **55**, 349 (2006).

[34] J. Rosti, X. Illa, J. Koivisto, and M. J. Alava, *Crackling noise and its dynamics in fracture of disordered media*, J. Phys. D: Appl. Phys. **42**, 214013 (2009).

[35] A. H. Patty, *significance Of Stress intensity Factor On Failure Behaviour Of Reinforced Concrete Beam (A case study of: Mode I Fracture)*. Int. j. eng. sci. invention **07**, 68 (2018).

[36] J. P. Sethna, *Course 6 Crackling noise and avalanches: Scaling, critical phenomena, and the renormalization group*, in J.-P. Bouchaud, M. Mézard and J. Dalibard eds., *Complex Systems*, Les Houches series **85**, 257 (Elsevier, Amsterdam, 2007).

[37] M. B. J. Meinders and T. V. Vliet, *Scaling of sound emission energy and fracture behavior of cellular solid foods*, Phys. Rev. E **77**, 036116 (2008).

[38] E. K. Salje and K. A. Dahmen, *Crackling Noise in Disordered Materials*, Annu. Rev. Condens. Matter Phys. **5**, 233 (2014).

[39] S. Santucci, L. Vanel, and S. Ciliberto, *Subcritical Statistics in Rupture of Fibrous Materials: Experiments and Model*, Phys. Rev. Lett. **93**, 095505 (2004).

[40] J. Dalege, et al., *Network Analysis on Attitudes: A Brief Tutorial*, Soc. Psychol. Personal. Sci. **8**, 528 (2017).

[41] A. -L. Barabási and E. Bonabeau, *Scale-free networks*, Sci. Am. **288**, 50 (2003).

[42] A.-L. Barabási, R. Albert, and H. Jeong, *Mean field theory for scale-free random networks.* Physica A. **272**, 173 (1999).

[43] S. Yook, H. Jeong, A. -L. Barabási, and Y. Tu, *Weighted Evolving Networks*, Phys. Rev. Lett. **86**, 5835 (2001).

[44] R. Albert, and A. -L, Barabási, *Statistical mechanics of complex networks*, Rev. Mod. Phys. **74**, 47 (2002).

[45] R. Albert, H. Jeong, and A. -L. Barabási, *Diameter of the World-Wide Web*, Nature **401**, 130 (1999).

[46] S. Redner, *How popular is your paper? An empirical study of the citation distribution*, Eur. Phys. J. B **4**, 131 (1998).

[47] M. E. J. Newman, et al., *Random graph models of social networks*, Proc. Natl. Acad. Sci. U. S. A. **99**, 2566 (2002).

[48] L. A. N. Amaral, et al., *Classes of small-world networks*, Proc. Natl. Acad. Sci. U. S. A. **97**, 11149 (2000).

[49] A. -L. Barabási and M. Pósfai, *Network science*, (Cambridge University Press, 2016).

[50] M. E. J. Newman, *Networks: an introduction*, (Oxford University press, USA, 2010).

[51] D. J. Watts, S. H. Strogatz, *Collective dynamics of 'small-world' networks*, Nature **393**, 440 (1998).

[52] A. Gautreau, A. Barrat, M. Barthelemy, *Microdynamics in stationary complex networks*, Proc. Natl. Acad. Sci. U. S. A. **106**, 8847 (2009).

[53] D. Pasten, F. Torres, B. A. Toledo, V. Munoz, J. Rogan and J. A. Valdivi, *Non-universal critical exponents in earthquake complex networks*, Physica A **491**, 445-452 (2018).

[54] S. Abe and N. Suzuki, *Scale-free network of earthquakes*, Europhys. Lett. **65**, 581 (2004).

[55] M. Baiesi and M. Paczuski, *Scale-free networks of earthquakes and aftershocks*, Phys. Rev. E **69**, 066106 (2004).

[56] A. Jiménez, K. Tiampo, A. Posadas , F. Luzón and R. Donner, *Analysis of complex networks associated to seismic clusters near the Itoiz reservoir dam*, Eur. Phys. J.: Spec. Top. **174**, 181 (2009).

[57] R. Korsnes, S. R. Souza, R. Donangelo, A. Hansen, M. Paczuski and K. Sneppen. *Scaling in fracture and refreezing of sea ice*, Physica A **331**, 291 (2004).

[58] J. N. Vevatne, E. Rimstad, S. M. Hope, R. Korsnes and A. Hansen, *Fracture networks in sea ice*, Front. Phys. **2**, (2014).

[59] L. D. Valdez, L. Shekhtman, C. E. L. Rocca, X. Zhang, S. V. Buldyrev, P. A. Trunfio, L. A. Braunstein and S. Havlin. *Cascading failures in complex networks.* J. Complex Netw. **8**, (2020)

[60] R. P. Satorras, et al., *Epidemic processes in complex networks*, Rev. Mod. Phys. **87**, 925 (2015).

[61] N. Jung, et al., *Avalanche size distribution of an integrate-and-fire neural model on complex networks*, Chaos **30**, 063118 (2020).

[62] S. Siddique, V. Volovoi, *Failure mechanisms of load-sharing complex systems*, Phys. Rev. E. **89**, 012816 (2014).

[63] J. Awrejcewicz and M. A. F. Sanjun, *Introduction to focus issue: recent advances in modeling complex systems: theory and applications*, Chaos **31**, 7 (2021).

[64] D. V. Stäger, N. A. M. Araújo and H. J. Herrmann, *Usage leading to an abrupt collapse of connectivity*, Phys. Rev. E. **90**, 042148 (2014).

[65] P. Crucitti, V. Latora and M. Marchiori. *Model for cascading failures in complex networks*, Phys. Rev. E **69**, 045104 (2004).

[66] A. E. Motter and Y. -C. Lai, *Cascade-based attacks on complex networks*, Phys. Rev. E **66**, 065102 (2002).

[67] R. Parshani, S. V. Buldyrev and S. Havlin, *Critical effect of dependency groups on the function of networks*, Proc. Natl. Acad. Sci. U. S. A. **108**, 1007 (2011).

[68] G. J. Baxter, S. N. Dorogovtsev, A. V. Goltsev, and J. F. F. Mendes, *Heterogeneous k-core versus bootstrap percolation on complex networks*, Phys. Rev. E **83**, 051134 (2011).

[69] G. J. Baxter, S. N. Dorogovtsev, A. V. Goltsev, and J. F. F. Mendes, *Bootstrap percolation on complex networks*, Phys. Rev. E **82**, 011103 (2010).

[70] A. Saichev and D. Sornette, *Andrade, Omori, and time-to-failure laws from thermal noise in material rupture*, Phys. Rev. E **71**, 016608 (2005).

[71] A. Guarino, et al., *An Experimental Test of the Critical Behaviour of Fracture Precursors*, Eur. Phys. J. B **6**, 13 (1998).

[72] X. Jiang, H. Liu, I. G. Main and E. K. H. Salje, *Predicting mining collapse: Superjerks and the appearance of record-breaking events in coal as collapse precursors*, Phys. Rev. E **96**, 023004 (2017).

[73] V. Kádár, G. Pál, and F. Kun, *Record statistics of bursts signals the onset of acceleration towards failure*, Sci. Rep. **10**, 2508 (2020).

[74] E. Bouchaud, *Scaling properties of cracks*. J. Phys. Condens. Mattter **9**, 4319 (1997).

[75] A. Buchel and J. P. Sethna, *Elastic Theory Has Zero Radius of Convergence*, Phys. Rev. Lett. **77**, 1520 (1996).

[76] S. Zapperi, P. Ray, H. E. Stanley and A. Vespignani, *Analysis of damage clusters in fracture processes*, Physica A **270**, 57 (1999).

[77] S. Zapperi, et al., *First-Order Transition in the Breakdown of Disordered Media*, Phys. Rev. Lett. **78**, 1408 (1997).

[78] F. Kun and H. J. Herrmann, *Damage development under gradual loading of composites*, J. Mater. Sci. **35**, 4685 (2000).

[79] C. Roy and S. S. Manna, *Brittle to quasi brittle transition in a compound fiber bundle*, Phys. Rev. E **100**, 012107 (2019).

[80] D. Sornette and J. Andersen, *Scaling with respect to disorder in time-to-failure*, Eur. Phys. J. B. **1**, 353 (1998).

[81] S. Roy and P. Ray, *Critical behavior in fiber bundle model: A study on brittle to quasi-brittle transition*, Europhys. Lett. **112**, 26004 (2015).

[82] Z. Danku, G. Ódor and F. Kun, *Avalanche dynamics in higher dimensional fiber bundle models*, Phys. Rev. E **98**, 042126 (2018).

[83] M. E. J. Newman and D. J. Walls, *Scaling and percolation in the small world network model*, Phys. Rev. E **60**, 7332 (1999).

[84] Y. M. Strelniker, S. Havlin and A. Bunde, *Fractals and Percolation. In: R. Meyers (Eds.), Encyclopedia of Complexity and Systems Science*, (Springer, New York, 2009).

[85] C. Moore and M. E. J. Newman, *Epidemics and percolation in small-world networks*, Phys. Rev. E. **61**, 5678 (2000).

[86] D. Stauffer and A. Aharony. *Introduction to percolation theory*, (Taylor and Francis, London, 1992).

[87] F. T. Peirce, *32—X.—Tensile Tests for Cotton Yarns v.—"The Weakest Link" Theorems on the Strength of Long and of Composite Specimens*, J. Text. Inst. Trans. **17**, 355 (1926).

[88] H. E. Daniels, *The statistical theory of the strength of bundles of threads. I*, Proc. R. Soc. Lond. A **183**, 405 (1945).

[89] M. Kloster, A. Hansen and P. C. Hammer, *Burst avalanches in solve-able models of fibrous materials*, Phys. Rev. E **56**, 2615 (1997).

[90] L. D. Arcangelis, A. Hansen, H. J. Herrmann, and S. Roux, *Scaling laws in fracture*, Phys. Rev. B **40**, 877 (1989).

[91] F. Kun, F. Raischel, R. C. Hidalgo, and H. J. Herrmann, *Modelling Critical and Catastrophic Phenomena in Geoscience: A Statistical Physics Approach*, Lecture Notes in Physics, edited by P. Bhattacharyya and B. K. Chakrabarti, (Springer-Verlag, Berlin, 2006) pp. 57–92.

[92] W. Weibull, *A statistical theory of the strength of materials*, Royal Swedish Academy of Engrg. Sci. Proc. **151**, 1 (1939).

[93] W. Weibull, *A statistical distribution function of wide applicability*, J. Appl. Mech. **18**, 293 (1951).

[94] J. V. Andersen, D. Sornette, and K. Leung, *Triciritical Behavior in Rupture Induced by Disorder*, Phys. Rev. Lett. **78**, 2140 (1997).

[95] A. Hansen, P. Hemmer, and S. Pradhan, *The Fiber Bundle Model: Modeling Failure in Materials, Statistical Physics of Fracture and Breakdown*, (Wiley, 2015).

[96] G. G. Batrouni, et al., *Heterogeneous interfacial failure between two elastic blocks*. Phys. Rev. E **65**, 036126 (2002).

[97] A. Delaplace, S. Roux, and G. Pijaudier-Cabot, *Damage cascade in a softening interface*. Int. J. Solids Struct. **36**, 1403 (1999).

[98] G. Batrouni and A. Hansen, *Fracture in Three-Dimensional Fuse Networks*, Phys. Rev. Lett. **80**, 325 (1998).

[99] W. A. Curtin, *Size Scaling of Strength in Heterogeneous Materials*, Phys. Rev. Lett. **80**, 1445 (1998).

[100] J. B. Gómez, D. Iñiguez, and A. F. Pacheco, *Solvable fracture Model with Local Load Transfer*, Phys. Rev. Lett. **71**, 380 (1993).

[101] A. Hansen and P. C. Hemmer, *Burst avalanches in bundles of fibers: Local versus global load-sharing*, Phys. Lett. A **184**, 394 (1994).

[102] S. Roy, S. Biswas, and P. Ray, *Modes of failure in disordered solids*, Phys. Rev. E **96**, 063003 (2017).

[103] D. Bonamy and E. Bouchaud, *Failure of heterogeneous materials: A dynamic phase transition?*, Phys. Rep. **498**, 1 (2011).

[104] U. S. Kachhwah and S. Mahesh, *Tough-brittle transition in the planar fracture of unidirectional fiber composites*, Phys. Rev. E **101**, 063002 (2020).

[105] D. Watts and S. Strogatz, *Collective dynamics of small-world networks*, Nature **393**, 440 (1998).

[106] D. Watts, *Networks dynamics and the Small World phenomenon*, Am. J. Sociol. **105**, 493 (1999).

[107] F. Kun, S. Zapperi and H. J. Herrmann, *Damage in fiber bundle models*, Eur. Phys. J. B **17**, 269 (2000).

[108] F. Raischel, F. Kun and H. J. Herrmann, *Local load sharing fiber bundles with a lower cutoff of strength disorder*, Phys. Rev. E **74**, 035104 (2006).

[109] M. E. J. Newman, *The Structure and Function of Complex Networks*, SIAM Rev. **45**, 167 (2003).

[110] L. Laurson, X. Illa, S. Santucci, K. T. Tallakstad, K. J. Maloy and M. J. Alava, *Evolution of the average avalanche shape with the universality class*, Nat. Commun. **4**, 4927 (2013).

[111] J. Gleeson and R. Durrett, *Temporal profiles of avalanches on networks*, Nat. Commun. **8**, 1227 (2017).